universität wien

# MASTERARBEIT

Titel der Masterarbeit

## Petrophysical properties of deformation bands in carbonate grainstones from micro computed tomography and cathodoluminescence measurements


Verfasser

Alexander Rath, Bakk. rer. nat.


angestrebter akademischer Grad

Master of Science (M.Sc.)

Wien, 2010

| | |
|---|---|
| Studienkennzahl lt. Studienblatt: | A 066 815 |
| Studienrichtung lt. Studienblatt: | Masterstudium Erdwissenschaften |
| Betreuer: | Univ. Prof. Mag. Dr. Bernhard Grasemann |

## *INTRODUCTION*

This diploma thesis combines microstructural, chemical and image analysis methods to analyze the relationship between deposition, deformation and cementation in Miocene limestones. The topic is about brittle fault structures called deformation bands occurring in the calcarenites of St. Margarethen, Burgenland. Erich Draganits discovered the deformation band in the Leitha Limestone and this was the initial input for working on this topic. The petrophysical properties of the deformation bands and the adjacent host rock were investigated, especially focussing on parameters (e.g.. porosity and permeability) which influence fluid flow in hydrocarbon reservoirs.

This work was accomplished under the supervision of Dr. Ulrike Exner and O. Univ. Prof. Bernhard Grasemann at the Department of Geodynamics and Sedimentology at the University of Vienna.

The aim of this study was to submit a paper in a journal for geosciences, to gain insight in writing a scientific paper and in the scientific work progress. This master thesis is in preparation to be submitted to the Bulletin American Association of Petroleum Geologists. The research focused on the methodology for acquiring petrophysical data and their results.

Due to this fact, the length of the master thesis is short, because of the guidelines for paper submission. In addition some acquired data were not included in this work; however, these results are presented in the appendix of this master thesis.

Conventional core analysis of drill cores and minipermeameter measurements were assessed at the laboratory of the OMV, LEP-FC, Vienna. These results provided a basis for further research and the idea of making this paper. First of all, neutron tomography data at the Institute of Atomic and Subatomic Physics were collected for a 3D visualization of the pore geometry and porosity. The obtained resolution of the data though was too low for further investigations. Instead, high resolution data - µCT measurements acquired at the Department of Anthropolgy, University of Vienna - were assessed to visualize and even quantify pore sizes and porosity. Different generations and chemical variations of cements in the calcarenites and cataclastic deformation of grains were investigated by the cathodoluminescence microscope. Further investigations on the electron microprobe were conducted to assess the

chemical composition of cement generations quantitatively and potentially identify the source of CL activation or distinguished between marine and meteoric cement types.

## *ABSTRACT*

In contrast to frictional faults and cataclasites in well consolidated and cemented sediments, lithologies with little or no diagenetic consolidation and high porosity develop deformation band type faults. Generally, deformation bands often form in well sorted fine to medium-grained sandstones before major porosity loss during diagenesis.

These deformation structures were studied at the Eastern border of the Eisenstadt Basin where deformation bands were found in Miocene calcarenites in a quarry near St. Margarethen (Eastern Austria). The Badenian Leithakalk (14-13 Ma) in the quarry mainly comprises bioclasts dominated by corallinacean debris and foraminifera.

The orientation of the deformation bands indicates E-W directed extensional kinematics which can be correlated to large scale horst and graben structures within the underlying basement and lower Miocene sedimentary rocks.

Thin section analysis of the same samples revealed a significantly lower amount of carbonatic cement within the deformation bands than in the undeformed limestone. However, cathodoluminescence depicts different types of deformation bands, on the one hand cataclastic deformation bands due to broken grains and no cementation and on the other hand disaggregation bands, due to grain rotation and translation and later cementation.

The permeability across selected deformation bands was measured with a minipermeameter. The deformation bands itself has almost zero permeability due to the decreased porosity. The permeability is reduced up to 3 magnitudes in contrast to the non-deformed rock fabric.

Three 3x3.5 cm sized drill core containing a deformation band each, were analyzed using X-ray micro-tomography with a spatial resolution of 30-40 microns. The pores outside the deformation band are 500-2000 microns in diameter, and show a well connected pore space. In contrast, the size of pores is strongly reduced within the deformation band to a maximum of 100 microns; the pores are clearly isolated and fill < 3 % of the volume, of the deformation band.

Generally, the Leithakalk shows a primary porosity of around 30 %, but within the deformation bands the porosity is reduced to ~1 %. A decrease of at least one

magnitude of porosity is shown. A broader deformation band >0.5 mm will also affect a porosity reduction adjacent to the deformation band.

Due to the detailed X-Ray micro-tomography data of the porosity within and outside the deformation bands, in combination with microstructural investigations, we are able to constrain the deformation mechanisms and relative timing of deformation with respect to the cementation of the limestone.

## *ZUSAMMENFASSUNG*

Im Gegensatz zu spröden Störungen und Kataklasiten in gut verfestigten und zementierten Sedimenten, werden in Gesteinen mit einer hohen Porosität und wenig bis gar keine Diagenese erfahren haben, Deformation Band - Störungen gebildet. Im Allgemeinen werden Deformation Bands oft in gut sortierten, fein- bis mittelkörnigen Sandsteinen vor großen Porositätsverlusten während der Diagenese gebildet.

Diese Deformationstrukturen wurden am Ostrand des Eisenstädter Beckens untersucht, wo Deformation Bands in miozänen Kalkareniten der Leithakalkformation des Steinbruchs St. Margarethen (Ostösterreich) aufgeschlossen sind. Der Badenische Leithakalk (14-13 Ma) im Steinbruch besteht hauptsächlich aus Bioklasten, die größtenteils aus Schutt von Corallinaceaen und Foraminiferen bestehen.

Die Lage der Deformation Bands zeigt eine E-W gerichtete extensionelle Kinematik, welche im Zusammenhang mit großmaßstäblichen Horst-Graben-Strukturen in dem unterliegenden Basement und den untermiozänen Sedimenten steht.

Dünnschliffanalysen der Proben zeigten einen deutlich niedrigeren Gehalt an karbonatischem Zement im Deformation Band als im nichtdeformierten Kalkstein. Die Kathodenlumineszenz zeigt jedoch unterschiedliche Arten von Deformation Bands, erstens: katklastische Deformation Bands aufgrund von zerbrochenen Körnern und keiner Zementation; zweitens: Disaggregations Bänder, welche sich durch Kornrotation/Korntranslation und spätere Zementation auszeichnen.

Die Permeabilität wurde mit einem Minipermeameter über ausgewählte Deformation Bands gemessen Die Deformation Bands selber haben fast keine Permeabilität aufgrund der verringerten Porosität. Die Permeabilität ist um 3 Größenordnungen im Vergleich zu der nichtdeformierten Gesteinsstruktur verringert.

Drei 3x3.5 cm große Bohrkerne, welche alle ein Deformation Band enthalten wurden mittles Röngten-Mikro-Computertomographie und einer räumlichen Auflösung von 30-40 Mikrometer gemessen. Die Poren außerhalb des Deformation Bands sind 500-2000 Mikrometer im Durchmesser groß und zeigen einen gut verbundenen Porenraum. Im Gegensatz dazu ist die Porengroße im Deformation Band stark reduziert mit einer maximalen Größe von 100 Mikrometer; Die Poren sind klar isoliert und füllen < 3 % des Volumens des Deformation Band.

Üblicherweise hat der Leithakalk eine primäre Porosität von ca. 30 %, aber in den Deformation Bands ist die Porosität auf ~1 % reduziert. Eine Reduktion von einer Größenordnung der Porosität ist messbar.

Aufgrund der Verwendung von detaillierten Röntgen-Mikro-Computertomographie Porositätsdaten im und neben dem Deformation Band, in Kombination mit mikrostrukturellen Untersuchungen, sind wir in der Lage den Deformationsmechanismus und eine relative Zeitberechnung der Deformation Bands unter Berücksichtigung der Zementation des Kalksteins zu bestimmen.

## *TABLE OF CONTENTS*

# Petrophysical properties of deformation bands in carbonate grainstones from micro computed tomography and cathodoluminescence measurements

---

## *INTRODUCTION*

Deformation bands in porous rocks are low-displacement deformation zones of millimeters to centimeters thickness that significantly reduce porosity and permeability (Fossen et al., 2007). The magnitude of permeability reduction is related to the petrophysical properties of the host sediment and may be quite variable even along an individual band (Torabi and Fossen, 2009).

Deformation bands were first described in Aeolian sandstones in Utah (Aydin, 1978; Aydin & Johnson, 1978); since then they were identified worldwide in porous sandstones (see Fossen, et al. 2007for a review). However, just some few examples of deformation bands were described from porous limestones (Tondi et al., 2006; Tondi 2007; Micarelli et al., 2006). In this paper we investigate deformation bands in porous calcarenites from the Eisenstadt-Sopron Basin, a southeastern satellite basin of the Vienna Basin (e.g. Royden, 1985). Samples were taken at a quarry, where the upper Badenian Leithakalk was deposited as a bioclast-dominated carbonate grainstone in shallow marine carbonate platforms aligned along the topographic high of the Rust ridge.

Using micro computed tomography (μCT), cathodoluminescence (CL) and minipermeameter measurements we analyze the deformation mechanisms in these deformation bands, thereby constraining the temporal and spatial relationship between deformation and cementation.

The resolution of X-ray computed tomography (CT) developed rapidly in the last decades. Earlier studies using conventional, usually medical CT-measurements to determine the porosity reduction in deformation bands provided a spatial resolution of roughly 200-500 μm (e.g. Antonelllini, 1994; Oglive et al., 2001; Alshibli, 2008),

where the tomographic images resolved general tendencies of pore size distribution on the mm-scale. In addition, conventional porosity and permeability measurements on drill cores and thin sections were employed to determine accurate values for these petrophysical parameters and thereby calibrate the CT data.

In contrast, micro computed tomography (μCT) scanners for non-medical applications permit the acquisition of data with a much higher spatial resolution, as a consequence of higher energy X-rays and increased measurement time (Ketcham & Carlson, 2001). In this study we present μCT measurements with a resolution of 30-40 μm, providing a 3D dataset of the spatial distribution of pores within and adjacent to the deformation bands. The standard processing and calibration of the μCT data was additionally enhanced by calibration of porosity from conventional thin sections. The investigated carbonate grainstones are particularly useful for this kind of measurement because they are porous, but solid rocks with a uniform density and mineralogy. The air-filled pore space provides the optimum contrast between rock and pore volume.

Additionally, changes in permeability across the deformation bands were quantified with minipermeameter measurements (Rotevatn, 2008; Torabi and Fossen, 2009).

Furthermore Cathodoluminescence (CL) thin section analysis was performed in order to determine the deformation mechanisms for the observed porosity and permeability reduction. In contrast to conventional optical microscopy, CL highlights cement seams which often contain different amounts of minor and trace elements than the biogenic grains of the host sediment due to changes in chemical composition of the pore fluid.

The various methods used in this study contribute to constrain the deformation history of the Leithakalk at the studied locality on the Rust Ridge, especially focusing on the relationship between deposition, cementation and formation of deformation bands.

## *GEOLOGICAL SETTING*

The quarry “Hummel” is situated 1 km east of St. Margarethen, Burgenland, Austria on the eastern border of the Eisenstadt-Sopron Basin (Fig. 1). This basin developed as a south-eastern satellite basin of the Vienna Basin during the middle Miocene along extensional normal- and strike-slip fault systems at the Eastern margin of the Alps (Decker et al., 2005).

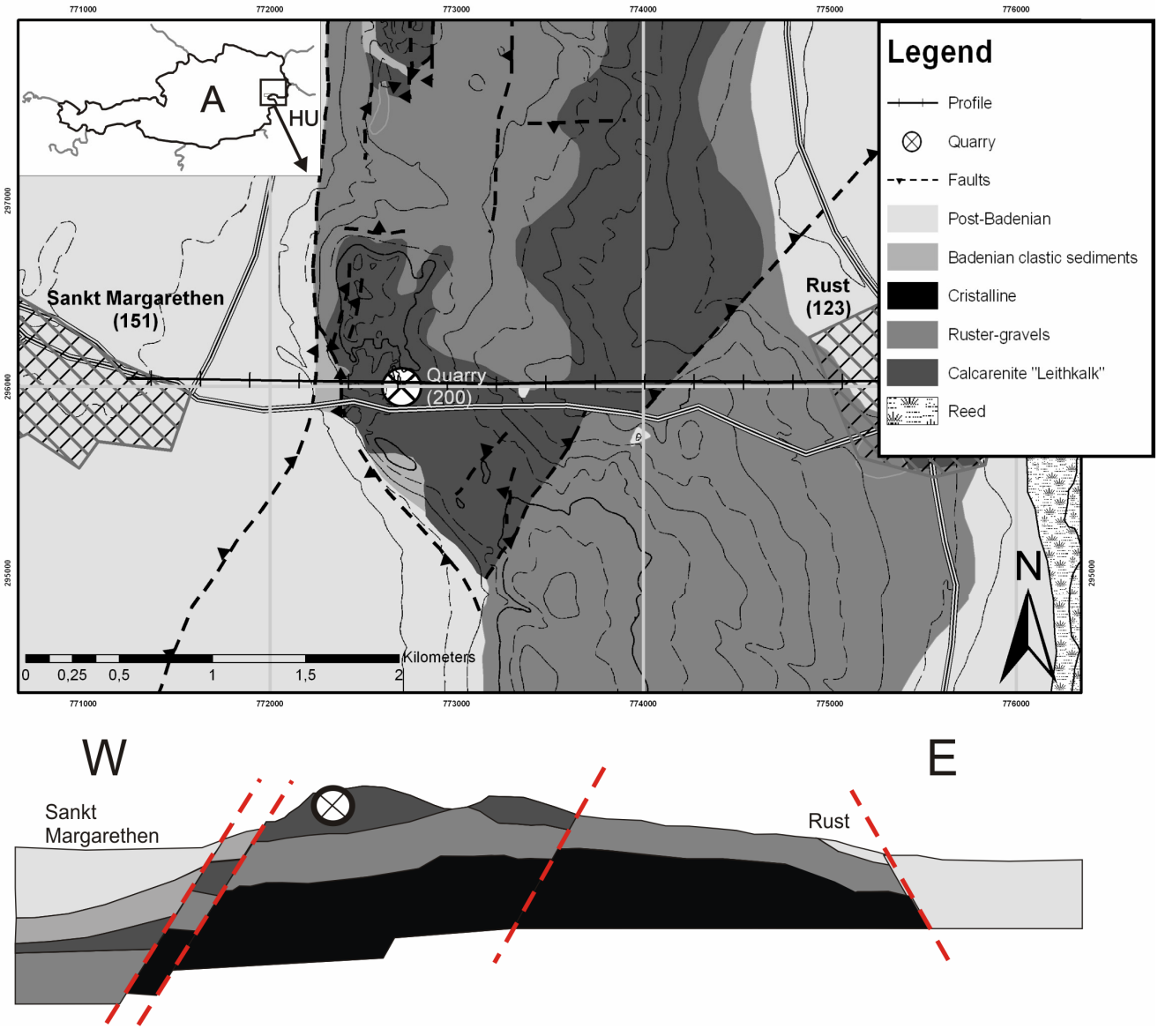


**Figure 1. Geographical and geological overview of the quarry Hummel. Schematic cross section striking W-E over the Rust ridge. (Strongly modified after Fuchs 1965)**

The basin started to form in the Karpatian, where fluvial sediments, mostly gravels, were deposited. During ongoing subsidence in the upper Badenian (14 to 13 Ma), elevated areas around the N-S trending Rust ridge evolved. A transgression in the Eisenstadt-Sopron basin during the Badenian (i.e. ~ Langhian, 16 to 13.6 Ma) resulted in minor, poorly diversified carbonate platform reefs which evolved on various shallow marine ridges (e.g. Leitha mountains, Rust ridge, Styrian basin). The reefs on these ridges were connected by channels/depressions in which clastic sediments (laminated marls, silty clays of the ”Badenian Tegel”) from delta fans along the basin margins were deposited. The driving forces for sedimentation of the Leitha limestone were storm events, which triggered transportation of carbonate sands and corallinacean debris of the reef to deeper levels (Schmid et al., 2001). The Leitha limestone in this study is of upper Badenian age (14 to 13 Ma); at least from the middle Sarmatian (i.e. ~ Serravallian, 13.6 to 11.6 Ma), horst and graben structures uplifted and exhumed the Rust range along N-S striking faults (Fig. 1), as documented by the deposition of fresh water clays in the westerly adjacent basin areas.

## *LITHOLOGY*

The Badenian Leitha limestone (Schmid et al., 2001.; Fuchs, 1965; Dullo, 1983) in the quarry can be classified as a grainstone (Dunham 1962), and mainly comprises bioclasts dominated by corallinacean debris, rhodolithes, oysters, pectinids and fragmented echinoids (Schmid et al., 2001). The Leitha limestone exhibits different kinds of cementation and diagenetic environments. Due to a strong heterogeneity of the varying reefs and diagenetic differences in the Leitha limestone a comparison with earlier sediment-petrographic studies (Dullo, 1983) is not attempted. Moreover, many stratigraphic and paleontological studies were published about the Leitha limestone (e.g. Schultz, 1993; Miklovský, 1998; Schmid et al., 2001). The maximum pore size is very heterogeneous varying from 0.5 mm to 3-4 mm (Fig. 2). The total porosity varies between 20-35 %. The Leitha limestone is characterized by a rather poor sorting and due to a medium grade of cementation, this high porosity sediment is remarkable stiff. This stone has been used for construction purposes for centuries due to its relatively easy quarrying and sawing properties, e.g. at the famous St. Stephan's Cathedral in Vienna (Rohatsch 2007).

In the quarry "Hummel" deformation bands are frequent, especially adjacent to a normal fault with some tens of meters of dip slip displacement. From the laminated Badenian marls underlying the Leitha limestones in a neighboring quarry a rich biogenic fauna is reported (Schmid et al 2001).


**Figure 2. Picture of an approximately 1.5 cm broad deformation band in the high porosity calcarenite. Within the deformation band the porosity is almost completely reduced due to grain rotation and crushing (loose block, Hummel quarry).**

## *STRUCTURAL DATA*

The bedding is nearly horizontal and slightly W-dipping. The oldest structures are several different deformation bands, which indicate a multi-stage evolution. Three different types of deformation bands were classified starting with the oldest (plots in Fig.3, after Laner, 2009)

- The first type is a conjugate set with normal fault behavior, dipping E-W.
- The second type dips E-W as well, but dips more steeply than the first type.
- The third type dips steeply N-S and fits to smaller faults located south in the quarry "Kummer" which is not part of this study (Schmid et al. 2001).

The second type varies from the first due to changing rheologic properties after ongoing solidification of the sediment and increasing overburden. Because of strain hardening and ongoing cementation of the deformation bands, brittle faults formed, which use the already existing deformation bands as initial planes (Aydin, 1978). These basin bordering N-S striking 60° westwards dipping faults do not show any superposition by younger faults. The throw on these faults is up to 200 m, as deduced from the geological map and cross section in (Fig. 1). The succession of deformation structures indicates a tectonic regime of ongoing E-W extension during the Badenian and Sarmatian.

The youngest structures are mode I joints and opening width of up to 5 meters, which are filled with laminated marls, soil and debris. Those joints are dipping vertically and are often in context with type 2 deformation bands. Their existence is interpreted as result of probably recent mass movements of the calcarenite towards the scarp in the west.

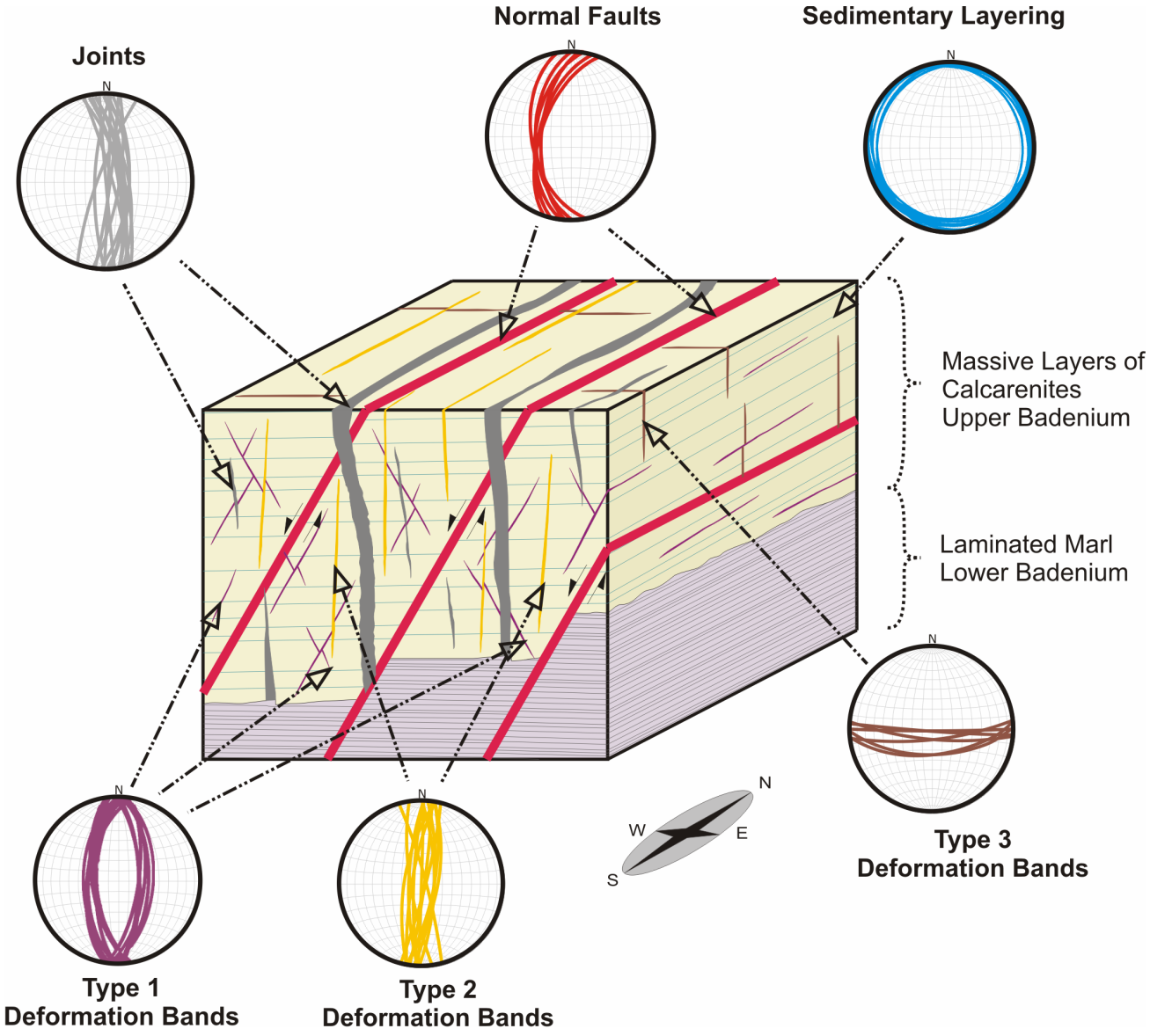


**Figure 3. 3D-diagram and stereoplots (equal area, lower hemisphere) of geological structures in the quarry Hummel. Three different deformation band types can be distinguished, as W-dipping normal fault udeveloping along the earlier deformation bands. All structures except for the west plunging normal faults just occur in the more rigid calcarenite and not in the underlying marl. (modified after Laner, 2009)**

## *METHODS*

All measurements were acquired at samples of the N-S striking type 1 and type 2 deformation bands in the Leitha limestone. All samples from sample Sm1 to sample Sm10 arise from the quarry "Hummel" in St. Margarethen, as well as 5 samples (M1-07 – M5-07) from Richard Laner bachelor thesis which he worked on. The samples are cuboid-formed loose blocks and it was not possible to receive orientated samples from the outcrop. However, knowing the exact orientations of the deformation bands is not necessary for finishing this work, due to the fact that this master thesis is based on the methodology for achieving petrophysical data and not about regional tectonics.
Porosity and permeability measurements were carried out using different laboratory, 3D- visualization and image analysis techniques.
Conventional core analysis of 3 cm broad drill cores including porosity (helium porosimetry) and permeability (gas permeability) were assessed. The helium porosity was measured to verify varying changes of porosity in the deformation bands and is a useful tool to calibrate the μCT data. In addition, the total porosity was calculated from the μCT data and a minipermeameter was used to calculate fluid flow preferences. Cathodoluminescence was assessed to investigate microstructures and cements in the deformation bands.
A total of 12 drill cores, 4 host rock samples and 8 drill cores containing a deformation band were studied using conventional core analysis.

### Permeability

Permeability was analyzed at the laboratory of OMV, LEP-FC, Vienna, using a stationary minipermeameter. In addition, gas permeability of all 12 drill cores was analyzed.
Eight cuboid samples, at a maximum size of 40 x 15 x 4 cm, were analyzed using a minipermeameter (Suboor et al., 1995; Goggin et al., 1988). The permeability was assessed by using nitrogen as measuring gas; a contact pressure of 8 bar was imposed on each measurement point with a tip radius of 2.4 mm. The minipermeameter measurements were assessed in a raster with a grid space of 1 cm, maximum 6 cm broad and 28 cm long, aligned perpendicular to the deformation bands to see

permeability fluctuations in and adjacent to the deformation band. The data were plotted and interpolated between the measuring points using MatLab.

## µCT

The used µCT scanner is a custom-made Viscom X8060 NDT hosted by the Department of Anthropology at the University of Vienna. Three 2.95 cm broad and up to 9.3 cm long drill cores were measured with the aim to visualize and quantify the pore volume with a high spatial resolution. Samples heights are for Sm1 3.77 cm, for Sm9 3.96 cm and for Sm1T11 9.3 cm.

The measuring setup for Sm1T11 was 110 kV and 250 mA; pre-filtering was achieved using a 0.25 mm copper plate. The exposition time was set to 1.5 seconds/image. The samples Sm1 and Sm9 were analyzed at 110 KV and 105 mA, a 0.4 mm copper target as a pre-filter was applied with an exposition time of 5 seconds/image.

From each drill core 3000 radiographic images were assessed to compute a 3D volumetric reconstruction. The resolution of the radiographic images of the drill cores is 25 µm, but varies from the actual resolution of the reconstructed slices, because of memory restrictions for measuring and visualization. As a result of the larger length of the drill core Sm1T11, the resolution is 40 µm, in contrast to the resolution of the shorter samples Sm1 and Sm9 of 30 µm (Fig. 4). These differences in resolution are the result of the technical limitation that a smaller sample size is related to a better spatial resolution. The resulting data are Tiff-formatted 16-bit grayscale image sequences, cropped at 0.1 cm distance from the rim in order to remove remnants of the beam hardening correction.

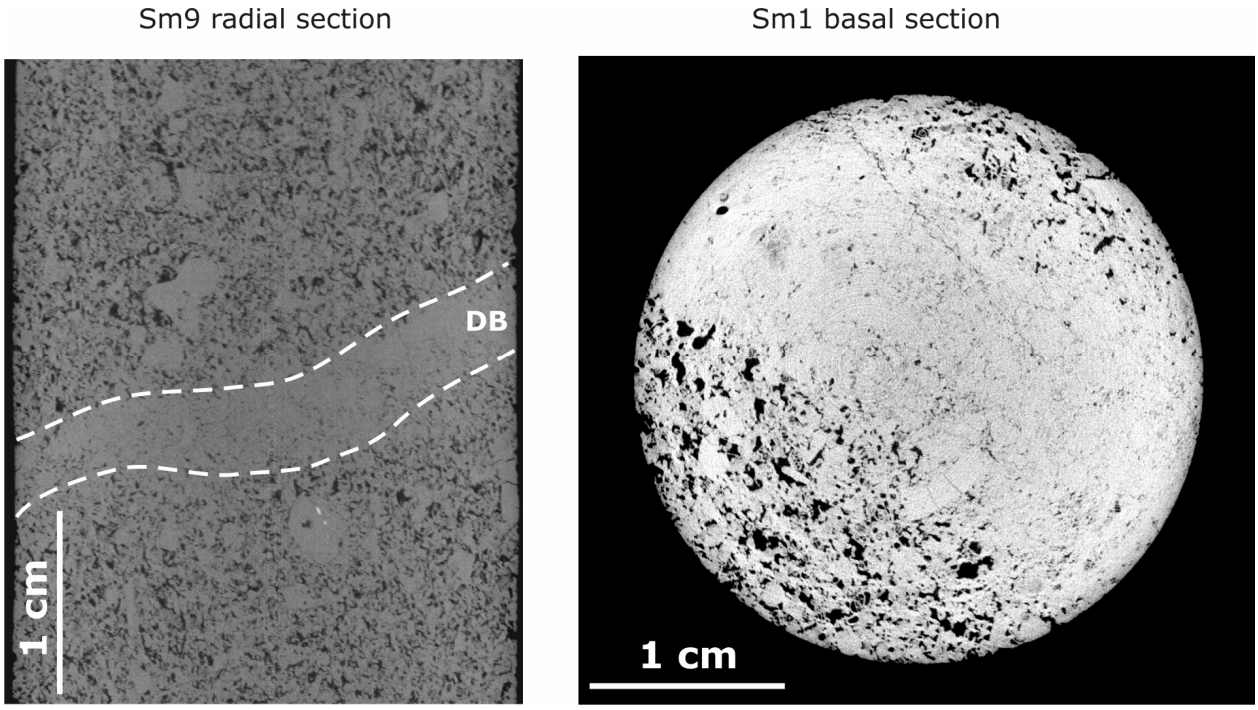


**Figure 4. µCT sections from two different drill cores. The resolution is 30 µm in both images. In both cases the greyish colors represent the rock and black air/pores. In the Sm9 radial section (left) the deformation band is slightly tilted and thinner than the one in the sample Sm1 (right). Small black spots representing porosities in the deformation band and well connected pore space and a high porosity (20 %) is distinguishable. The deformation band in sample Sm1 is up to 1.8 cm broad and due to the high-resolution data even small mode I opening cracks can be identified crosscutting the deformation band. These small cracks increase permeability and porosity of the deformation band.**

The calibration of the µCT data was carried out using 2 different methods. The first calibration method results from the helium porosimetry data of the measured drill cores, while the second method is based on thin sections of the drilled cores. Theses thin sections were impregnated with blue raisin to calculate the porosity with image analysis software packages (Adobe Photoshop CS4 and ImageJ). The thin sections were identified in the slices of the µCT-data and the gray value can be identified by thresholding the gray value to fit the total porosity. Using this gray value the whole core porosity could be determined from the µCT data using the commercial CT visualization software Amira. The same procedure was done the other way round, taking the results of the helium porosimetry and calculating the gray value for the whole core and the slice wherein the thin section is located, to determine variation of those two calibration techniques.

Knowing the right gray value of each drill core, certain sub-volumes were extracted, with varying total volumes resulting from different image resolutions and pore sizes.

The sub-volumes were aligned in a profile next to each other and each was calculated. Per sample 5 such profiles were measured across the deformation band to differentiate porosity changes across deformation bands. The data of the profiles were averaged for statistical reasons.

One example for slightly shifted data can be beam hardening, which causes the edges of an object to appear brighter than the center, even if the material is homogeneous. As the beam passes through the scanned object, the mean beam X-ray energy increases or "hardens" (Ketcham et al. 2001). The beam hardening correction was performed using DigiObs Software. Ring artifacts are often another undesirable source of error in μCT data, which depict partial or full circles centered on the rotational axis, disturbing the data due to increased gray values (Ketcham et al. 2001). In our case just one of our three cores has strong ring artifacts, but those are located in an area in the core, which can be disregarded, so that this error is in this special case negligible.

## Cathodoluminescence

Three polished thin sections were analyzed using a LUMIC HC5-LM hot-cathodoluminescence microscope at the Department of Lithospheric Research, University of Vienna. Snapshots were taken at 14 KV and 5-7 mA and an exposition time of 971 ms. Due to color variations resulting from different chemical compositions of the cements and the bioclasts, the amount of cement can be segmented and measured using Photoshop CS4 and ImageJ.

## *RESULTS*

The analysis of thin sections with an optical microscope did not provide clear indicators for cataclastic deformation. Instead, rotation and translation of bioclasts indicates ductile deformation within in the deformation bands. The long axes of ellipsoidal bioclasts (e.g. foraminifera, Fig. 5) are aligned parallel to the deformation bands, and show a gradual decrease in rotation towards the undisturbed host rock. Generally, a medium grade of cementation and a high porosity is observable.

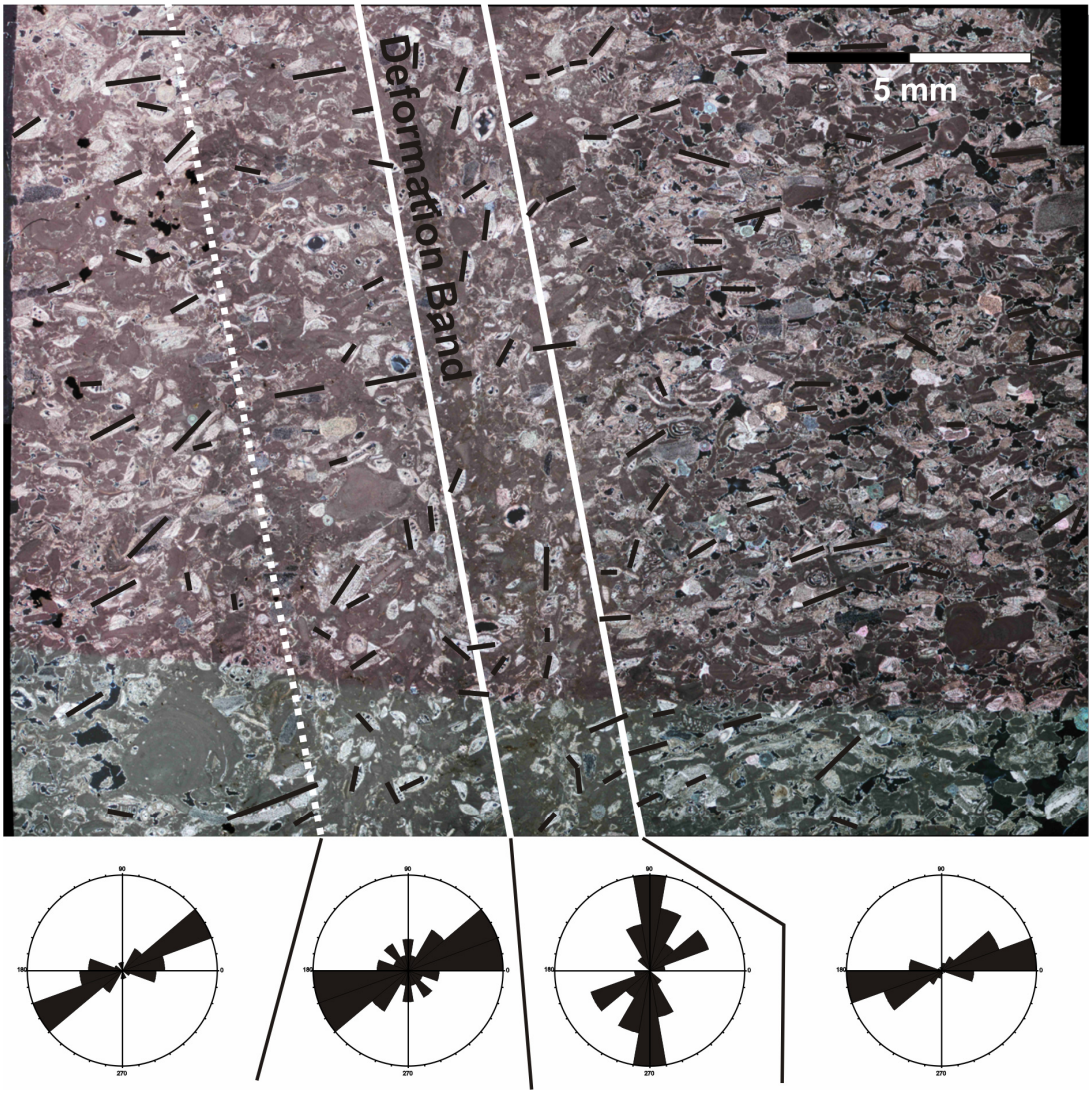


**Figure 5. Thin section of the calcarenite (M1-07), cut by a type 2 deformation band, including rose diagrams of the alignment of foraminifers and other bioclasts. On the right side and on the far left side the bioclasts are oriented preferably parallel to the sedimentary bedding (subhorizontal in the orientation diagram). Within the core of the deformation band foraminifera are aligned parallel to the shearing direction.**

In contrast to optical microscope analysis, cathodoluminescence shows evidence of grain crushing and grain size reduction. In general each pore is more or less cementated even though the amount and cement type varies. The analysis concluded that three different zones of compaction and cementation can be classified (Fig.6).

Zone 1: This zone is strongly compacted and almost free from cement and the porosity is reduced to lower than 2 %. However, in the small pores, some cement composed exclusively of calcite can be observed. In some few cement grains, twining lamellae indicate deformation of the crystal lattice. As far as grain size reduction and cracking of grains is concerned, almost exclusively corallinacean parts but rarely foraminifera are affected. Small opening mode I joints can occur, which are filled by very small cement crystals. Cathodoluminescence images appear darker than the other two zones due to the lower amount of cement.

Zone 2: The second zone is compacted, but not in the extent of Zone 1 but exhibits extensive grain crushing. The porosity is much higher (approx. 15 %) and different cements and tangential grain contacts can be observed. Cements between the grain contacts leads to the conclusion that the deformation took place after first cementation. In addition twining lamellae is also in this zone observable. The whole zone displays a much brighter (orange) color than in the Zone 1 due to a higher amount of cements.

Zone 3: In Zone 3, no signs of deformation structures were detected and the porosity ranges from 20 % to 30 %. Between the point contacts of the grains no cement is located. A syntaxial cement is observed, overgrowing preferably echinoid fragments; the absence of this type of cement in the aforementioned zones suggests a generation after the formation of the deformation bands.

The evolution of a Zone 1 is significantly related to thicker deformation bands, in contrast to thinner deformation bands (~<0.5 mm) where only Zone 2 is developed. The amount of cement was calculated from segmented CL images, providing a 1.5 times higher amount of cement in Zone 3 compared to Zone 3. These observations indicate that the reduced pore volume in the deformation bands is correlated with a decrease in fluid flow and lower cementation. In the host rock (Zone 3), the amount of cement is approximately 5 times higher than in Zone 1.

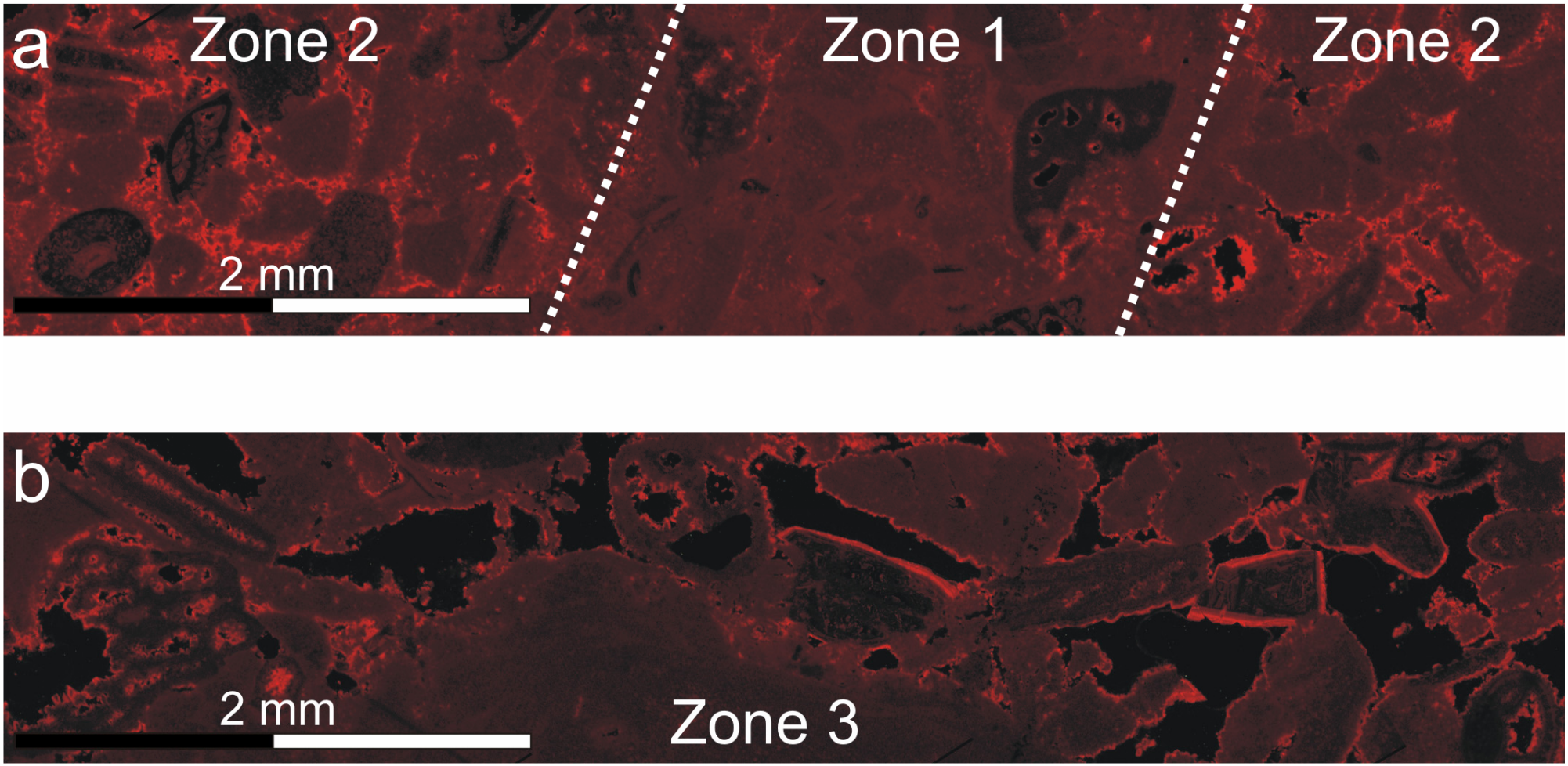


**Figure 6. Cathodoluminescence microscope images of sample Sm8n a) A region outside a big deformation band, which can be divided into two separate zones. Zone 1 is compacted and only few broken grains and almost no cement (bright orange colors) can be seen. In contrast, zone 2 shows a higher porosity and a much higher amount of cement. b) An image of the non-deformed rock with a high porosity and large grains. Furthermore, an additional generation of cement, i.e. syntaxial overgrowth of echinoid fragments characterized by straight edges, occurs in addition to the earlier dogtooth cement.**

## Minipermeameter – Permeability

Minipermeameter results show a decrease of permeability of up to 4 magnitudes, depending on the pore size of the non-deformed host sediment. In general at least 2.5 magnitudes of permeability difference are observed between the deformation band (0.2 – 10 mD) and non-deformed rock (60 - 7976 mD). In detail, the permeability in strongly deformed bands, showing cataclasis and clays, is reduced to 0.2 mD in contrast to typical deformation bands in which the permeability is reduced to 1 – 10 mD. The permeabilities in the non-deformed rock are very heterogeneous due to varying pores size. In some samples the permeability is increased adjacent to the deformation band and decreases again at further distance (Fig. 7). The increase of permeability is observed to be stronger and shows a higher gradient on one side of a deformation band than on the other. 2 out of the 8 measurements did not supply reliable data, one due to weathering and one due to rough sawing, resulting in unrealistic low permeability-values.

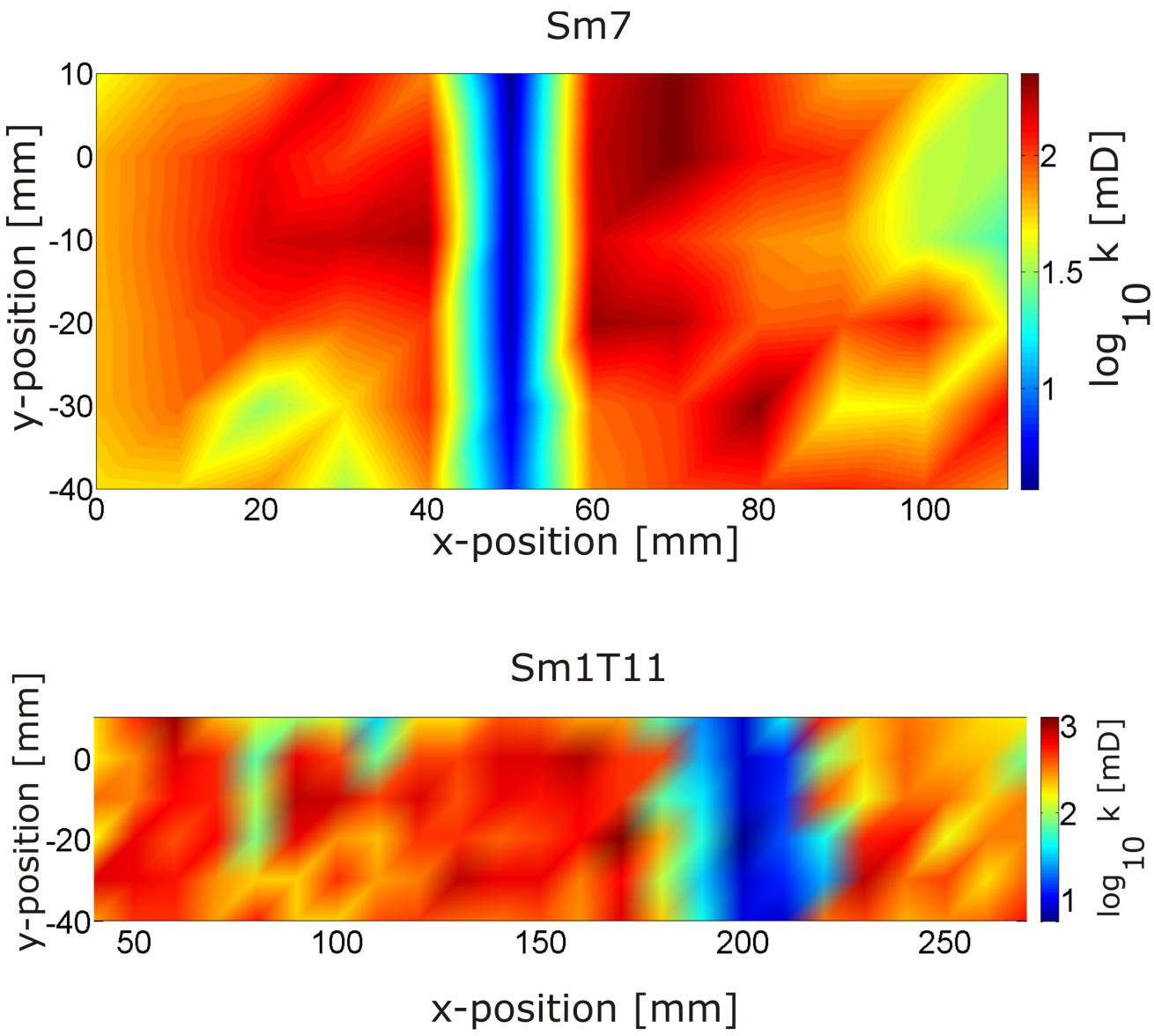


**Figure 7. The data points of the minipermeameter measurements were interpolated using MatLab (Algorithm: shading interp) to obtain a permeability map. The data points are aligned in a grid of 10 mm distance from each data point. The deformation band is colored in blue, indicating the lowest permeability. The highest values of permeability are red and are often situated right next to the deformation band. The permeability differences between the deformation band and the highest permeability are in the sample Sm7 up to 2.5 magnitudes. Sample Sm1T11 is the same as the sample of µCT data. Here the difference of permeability is up to 3 magnitudes.**

## Porosity

The porosity was measured with two different methods - helium porosimetry and the calculated porosity profiles from the µCT data representing different results. The result of the helium porosimetry is the effective porosity, while in contrast the µCT data provide the absolute porosity.

The helium porosimetry measurements of the drill cores from the host rock provide an effective porosity of up to 30.5 %. Cores containing a deformation band show an effective porosity reduced to 15 - 20 %.

As far as the µCT porosity is concerned, a calibration had to be assessed to determine the best fitting gray value as a threshold value for the distinction between air-filled pore space and solid rock. The calibration revealed large differences in the results of the thin section and the effective porosity data deduced from drill core measurements. The calibration of the drill core Sm1T11 fitted best, reporting differences of 2 percentage points of porosity between both techniques. This core is the longest, 9.3 cm in length and 2.95 cm in diameter, with a resolution of 40 µm. The other two cores show high differences between the two calibration methods of up to 9 % porosity.

Finally the thin sections were used as a calibration tool, because of the fact that this calibration is most reliable. Sample Sm1T11 (Fig. 8) is crossed perpendicular to the drilling direction by a 1 cm thick deformation band, in which the porosity is reduced down to 1.1 % in the deformation band, whereas the porosity is 35 % in the non-deformed rock. Calculated sub-volumes from which the porosities were obtained have a total volume of 65.8 $mm^3$. A decrease of porosity is seen in a 5 cm broad zone and levels off to 30 % further away. A comparison to the minipermeameter measurements is possible and the observed permeability is strongly reduced in a 3 cm broad zone in contrast to µCT results, where a decrease of porosity in a just 1 cm broad zone is observed. Unfortunately a decrease of porosity further away from the deformation bands, as seen in permeability measurements, could not be observed due to limiting length of the drill core.

Sample Sm9 (Fig. 8) depicts a 0.4 cm broad slightly tilted deformation band which is characterized by a zone of small pore sizes. The calculated sub-volumes are 27.8 $mm^3$ in size. The total porosity in the non-deformed rock is up to 22.2 % while it is reduced down to 2.1 % in the deformation band. The decrease of porosity is limited to an area

of 13 mm size, even though the deformation bands look broader. Due to fact that sample Sm9 is crossed by a thinner deformation band, the porosity further away was calculated and stays constant at about 20 %, indicating no porosity decrease in contrast to the permeability measurements of the same sample.

In sample Sm1 a 1.7 cm broad deformation band strikes parallel to the drilling direction and the porosity profiles are aligned in the deformation band to see variation of deformation band porosity. The total volume of the sub-volumes is just 11.8 $mm^3$, due to very small pores resulting from the dense compaction of the deformation band. The porosity varies from 0.3 % to 1.9 % in the deformation band resulting in a small increase in the middle of the deformation band. This slight increase represents a small opening mode I joint which is located in a Zone 1 of a deformation band.

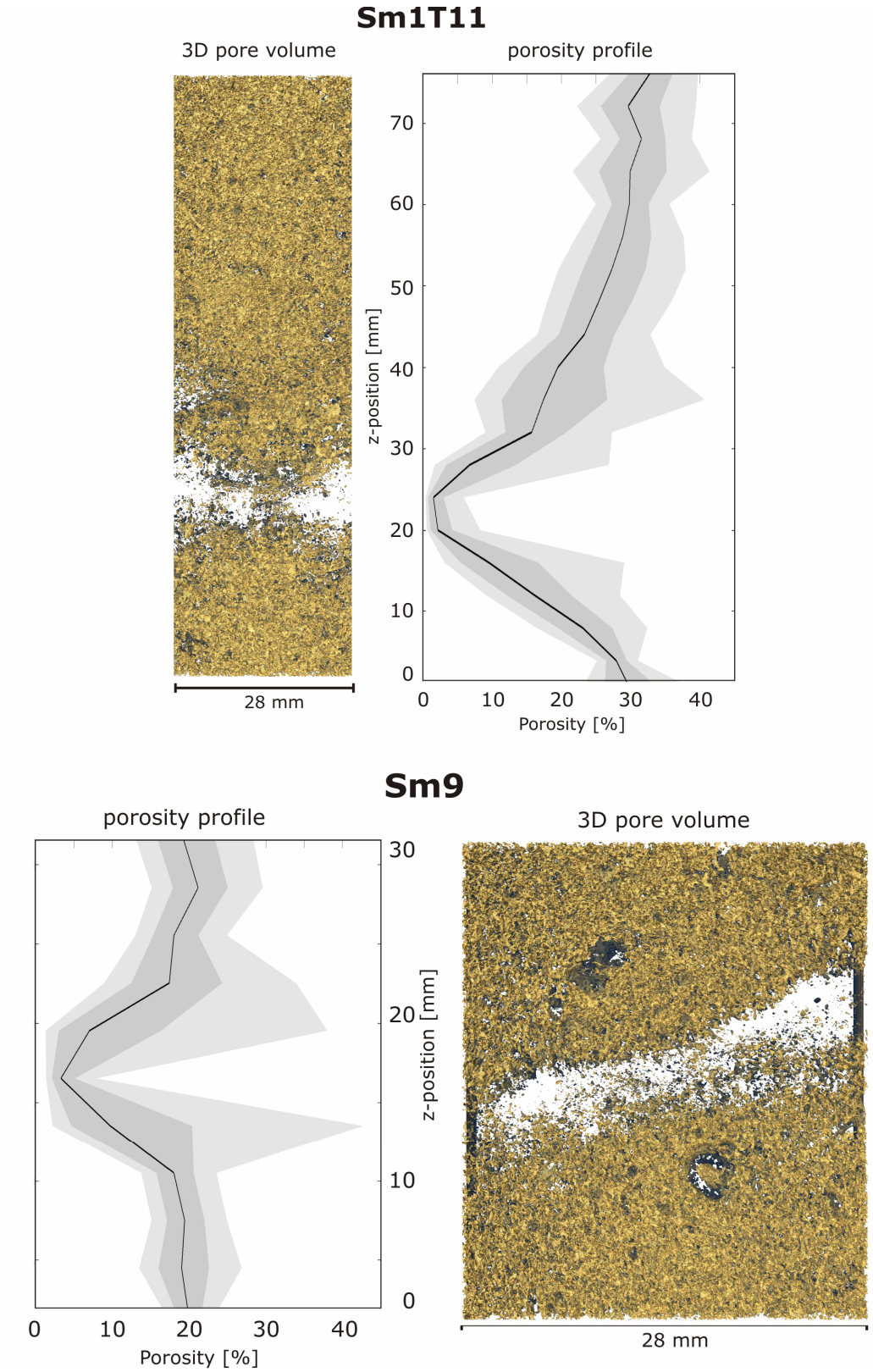


**Figure 8. 3D- models of the pore space and corresponding porosity profile of the samples Sm1T11 and Sm9. The black lines in the profiles represent the mean values of 5 profiles, the dark gray area marks 68 % (average + std.dev.) and the light gray 95 % (average+ 2*std.dev.) of all values. Sm1T11 displays a drill core which is crossed by an 1 cm broad deformation band and presents a porosity reduction not only in deformation band, but also up to 2 cm away from this zone. Compared to Sm9, where just a 0.4 cm broad deformation band is located, the porosity decrease is exclusively observed within the core of the deformation band.**

# *DISCUSSION*

## Diagenetic model and evolution of the deformation bands

In general there are several indicators how the Leitha limestone and the deformation bands within evolved. The evolution of a deformation band is directly connected to the diagenetic model. The deformation bands formed synsedimentary after the grains were transported due to storm events to deeper levels. Schmid et al. (2001) propose a frequent occurrence of earthquakes in this area related to E-W extension, which could be an explanation for the evolution of these early bands. Due to the fact that Zone 1 contains no micritic cement the evolution of deformation bands occurred shortly after deposition before the precipitation of micritic cement. Some remnants of aragonite (micritic) are observable in the investigated thin sections, which may be associated with vadose leaching (Dullo, 1983). Replacing most of this marine micritic cement, a coarser grained dog tooth cement developed. Zone 2 deformation bands were formed during and after precipitation of dog tooth cements because they are trapped between tangential grain contacts. At a later stage, probably related to a sea level rise (Schmid et al., 2001), syntaxial calcite overgrowth developed mainly along echinoderm fragments in a shallow marine environment. However these are only observed in the non-deformed rock, and give evidence for reduced fluid flow in the deformation bands. Generally, the cementation in such an environment is a fast process and is an evidence for a very early evolution of the deformation bands. Due to ongoing E-W extension normal faults with cataclastic slip surfaces evolved from deformation bands due to strain hardening, documenting the uplifting of the Rust Ridge.

## Deformation band properties and their role on fluid flow

The deformation bands observed are a mixture of cataclastic and disaggregation bands (Fossen, 2007). If a Zone 1 is developed it shows disaggregation of grains, without significant fracturing of grains or cement seams. In contrast, Zone 2 shows clear evidence of cataclastic deformation, as both bioclasts and carbonate cements are

fractured. Deformation band are precursor structures for normal faults (Micarelli 2006), indicating strain hardening behaviour. Evidences for these time steps from the evolution of deformation bands to faulting were found in the investigated samples.

Due to the strain hardening porosity and permeability in the deformation band is reduced in a narrow zone to a minimum. This decrease depends however on the deformation band width, which is directly proportional to the compaction and deformation strength. The wider the deformation band, the larger the decrease of porosity and permeability is. The initially developing disaggregation bands (Zone 1) are further deformed after the precipitation of dogtooth cements around the individual grains. The Zone 2 deformation bands thus show evidence of cataclastic deformation of bioclasts and cement seams. Beyond the tips of Zone 1 deformation bands, on in new sites of localization, only Zone 2 deformation bands are observed. The minipermeameter measurements revealed higher permeabilities adjacent to the deformation band. This may be interpreted as the damage zone of a cataclastic deformation band; alternatively, preferred fluid flow and dissolution subparallel to the bands may have created a secondary porosity along the bands. However, the porosity measurements from the μCT are not proving this assumption. Thin deformation bands (<0.4 cm) porosity results show a decrease of porosity just in the deformation band and no strong fluctuations further away. Thicker bands are affecting also adjacent areas resulting in a porosity-decrease of the surrounding areas.

To summarize the petrophysical properties these structures can be an effective lateral seal for hydrocarbons (Micarelli, 2006; Antonellini & Aydin, 1994, 1995; Shipton et al., 2001) due to strong decrease of permeability of up to 4 magnitudes and the decrease of porosity in a deformation band down to 1 %. The permeability is in fact increased next to the deformation band where fluid can accumulate but the deformation band itself is almost impermeable.

Moreover deformation bands are often allocated near larger brittle deformation structures being structures often of strain softening and a high fluid flow. The occurrence of many sets of conjugated deformation bands as a damage zone of a fault (Micarelli, 2006; Shipton et al. 2001) can affect fluid flow problems in reservoirs.

## µCT - Porosity

The µCT is a powerful tool to investigate high-porosity rocks in a nondestructive way. For calibration the method using thin sections was applied, because of a higher accuracy in contrast to the core analysis. The drill core porosity result reflects the effective porosity, while µCT assesses the absolute porosity. The calculation of effective porosity or permeability from µCT data is a non trivial task, involving either empirical equations and/or numerical modeling of fluid flow (e.g. Torabi & Fossen, 2009). For this reason and due the beam hardening correction varying results in the two calibration techniques are possible. One disadvantage is the partial volume effect, in which a single voxel can contain several different materials, resulting in an averaged gray value. To reduce this error, high resolution 3D models are required. From such accurate 3D porosity models, permeability and fluid pressure can be calculated.

## *CONCLUSIONS*

Cathodoluminescence and μCT were used to study deformation bands in high porosity calcarenites on the Rust ridge in Austria. We developed a diagenetic model for the evolution of the synsedimentary deformation bands. The first deformation bands evolved synsedimentary, cementation started and further deformation bands evolved. During to ongoing E-W extension on the Rust ridge the deformation bands did not accommodate further deformation and normal faults formed, using the deformation bands as initiation sites.

The investigated deformation bands show strain hardening behavior and are severe fluid flow barriers in contrast to the normal faults. Due to the strongly decrease in permeability and porosity, sets of deformation band can produce fluid flow problems in hydrocarbon reservoirs. The fluid flow is reduced up to 4 orders of magnitude the porosities at least 1 magnitude. The initial disaggregation bands evolve to cataclastic deformation band due to continuing cementation of the calcarenite. Our data indicate that μCT analysis is suitable for analyzing porosity distribution in high-porosity sediments and is capable of being a basis for highly sophisticated permeability and fluid pressure models. Due to the high resolution, small pores and pore connectivity down to approximately 25 μm in diameter can be analyzed.

## *REFERENCES*


Alshibli, K. A., and A. Hasan, 2008, Spatial variation of void ratio and shear band thickness in sand using X-ray computed tomography: Geotechnique, v. 58, p. 249-257.

Antonellini, M. A., and A. Aydin, 1995, Effect of faulting on fluid flow in porous sandstones: petrophysical properties: AAPG Bulletin, v. 78, p. 642-671.

Antonellini, M. A., A. Aydin, D. D. Pollard, and P. D´Onfro, 1994, Petrophysical Study of Faults in Sandstone Using Petrographic Image Analysis and X-ray Computerized Tomography: Pure and Applied Geophysics, v. 143, p. 181-201.

Aydin, A., 1978, Small faults formed as deformation bands in sandstone: Pure and Applied Geophysics, v. 116, p. 913-930.

Aydin, A., and A. M. Johnson, 1978, Development of Faults as Zones of Deformation Bands and as Slip Surfaces in Sandstone: Pure and Applied Geophysics, v. 116, p. 931-942.

Decker, K., H. Peresson, and R. Hinsch, 2005, Active tectonics and Quaternary basin formation along the Vienna Basin Transform fault: Quaternary Science Reviews, v. 24, p. 307-322.

Dullo, W.-C., 1983, Fossildiagenese im miozänen Leitha-Kalk der Paratethys von Österreich: Ein Beispiel für Faunenverschiebungen durch Diageneseunterschiede (Diagenesis of Fossils of the Miocene Leitha Limestone of the Paratethys, Austria: An example for Faunal Modifications Due to Changing Diagentic Environments: Facies, v. 8, p. 1-112.

Dunham, R. J., 1962, Classification of carbonate rocks according to depositional texture: AAPG Memoir, v. 1, p. 108-121.

Fossen, H., R. A. Schultz, Z. K. Shipton, and K. Mair, 2007, Deformation bands in sandstone: a review: Journal of the Geological Society, v. 164, p. 755-769.

Fuchs, W., 1965, Geologie des Ruster Berglandes (Burgenland): Jahrbuch der Geologischen Bundesanstalt, v. 1085, p. 155-194.

Goggin, D. J., R. L. Thrasher, and L. W. Lake, 1988, A theoretical and experimental analysis of minipermeameter response including gas slippage and high velocity flow effects: In Situ, v. 12, p. 79-116.

Ketcham, R. A., and W. D. Carlson, 2001, Acquisition, optimization and interpretation of X-ray computed tomographic imagery: applications to the geosciences: Computers & Geosciences, v. 27, p. 381-400.

Laner, R., 2009, Deformation Bands in neogenen Kalksandsteinen des Eisenstädter Beckens (St. Margarethen, Burgenland): Bakkalaureatsarbeit, Universität Wien, 37 p.

Micarelli, L., A. Benedicto, and C. A. J. Wibberley, 2006, Structural evolution and permeability of normal fault zones in highly porous carbonate rocks: Journal of Structural Geology, v. 28, p. 1214-1227.

Miklovský, J., 1998, A new loon (Aves: Gaviidae) from the middle Miocene of Austria.: Ann. Naturhist. Mus. Wien, v. 99A, p. 331-339.

Ogilvie, S. R., and P. W. J. Glover, 2001, The petrophysical properties of deformation bands in relation to their microstructure: Earth and Planetary Science Letters, v. 193, p. 129-142.

Ogilvie, S. R., J. M. Orribo, and P. W. J. Glover, 2001, The influence of deformation bands upon fluid flow using profile permeametry and positron emmission tomography: Geophysical Research Letters, v. 28, p. 61-64.

Rohatsch, A., 2007, Stephansdom: Gottes ewige Baustelle: Wanderung in die Erdgeschichte, v. 22, p. 22-25.

Rotevatn, A., A. Torabi, H. Fossen, and A. Braathen, 2008, Slipped deformation bands: a new type of cataclastic deformation bands in Western Sinai, Suez Rift, Egypt: Journal of Structural Geology, v. 30.

Royden, L. H., 1985, The Vienna Basin: A thin-skinned pull-apart basin, in K. T. Biddle, and N. Christie-Blick, eds., Strike-slip deformation, basin formation, and sedimentation: SEPM Special Publications, v. 37, p. 319-338.

Schmid, P. H., M. Harzhauser, and A. Kroh, 2001, Hypoxic Events on a Middle Miocene Carbonate Platform of the Central Paratethys (Austria, Badenian, 14 Ma): Ann. Naturhist. Mus. Wien, v. 102A, p. 1-50.

Schultz, O., 1993, Der Nachweis von Scorpaena s.s. (Pisces, Teleostei) im Badenian von St. Margarethen, Burgenland, Österreich. Revision von Scorpaena prior HECKEL in HECKEL & KNER, 1861.: Ann. Naturhist. Mus. Wien, v. 95A, p. 127-177.

Shipton, Z. K., and P. A. Cowie, 2001, Damage zone and slip-surface evolution over m to km scales in high-porosity Navajo sandstone, Utah: Journal of Structural Geology, v. 23, p. 1825-1844.

Suboor, M. A., and J. P. Heller, 1995, Minipermeameter characteristics critical to its use: In Situ, v. 19, p. 225-248.

Tondi, E., M. A. Antonellini, A. Aydin, L. Marchegiani, and G. Cello, 2006, The role of deformation bands, stylolites and sheared stylolites in fault development in carbonate grainstones of Majella Moumtain, Italy: Journal of Structural Geology, v. 28, p. 376-391.

Torabi, A., and H. Fossen, 2009, Spatial variation of microstructure and petrophysical properties along deformation bands in reservoir sandstones: AAPG Bulletin, v. 93, p. 919-938.

# *APPENDIX*

## Further methods

Of a split sample BSE images were obtained at the Natural History Museum, at the Department of Mineralogy to investigate grain crushing and cements in the deformation bands. A small deformation band less than 0.5 cm broad was analyzed but no grain crushing in the deformation band could be observed. The observed cements were dogtooth cements, cements with a rhomboedric structure and syntaxial cements – on which small cement crystals grow.

6 thin sections were analyzed under the electron microprobe for the investigation of porosity, grain crushing, chemical differences in the mineralogy and for chemical variation of the different cements were element maps of 2 pores obtained. The element maps of the 2 pores were measured to enhance and compare the information of the cathodoluminescence.

The electron microprobe revealed the same results as the split sample BSE images showing no cataclastic deformation in the deformation bands. However the inner structures of the pores and micropores were of special interest in the study and revealed many micropores and few macropores in the deformation bands, in contrast to the host rock. These small pores highlight a technical problem of the μCT. The μCT-data resolution is 30 μm but the micropores are smaller than 10 μm resulting in a grayvalue which is not taken into account in the total porosity calculation. Electron microprobe overview images, from the deformation band, the host rock and a transition zone were processes with ImageJ to calculate the porosity from them. The results show a total porosity of 31 % to 24 % in the host rock and the porosity in the transition zone depends on the total porosity of the host rock and varies between 8 % and 17 %. The total porosity inside the deformation band is reduced to 2 - 5 %.

In general huge differences in pore size and total porosity between deformation band and host rock could be observed. The calculated porosity revealed similar results as the drill cores.

## SEM Images

### *BSE image of a split sample*

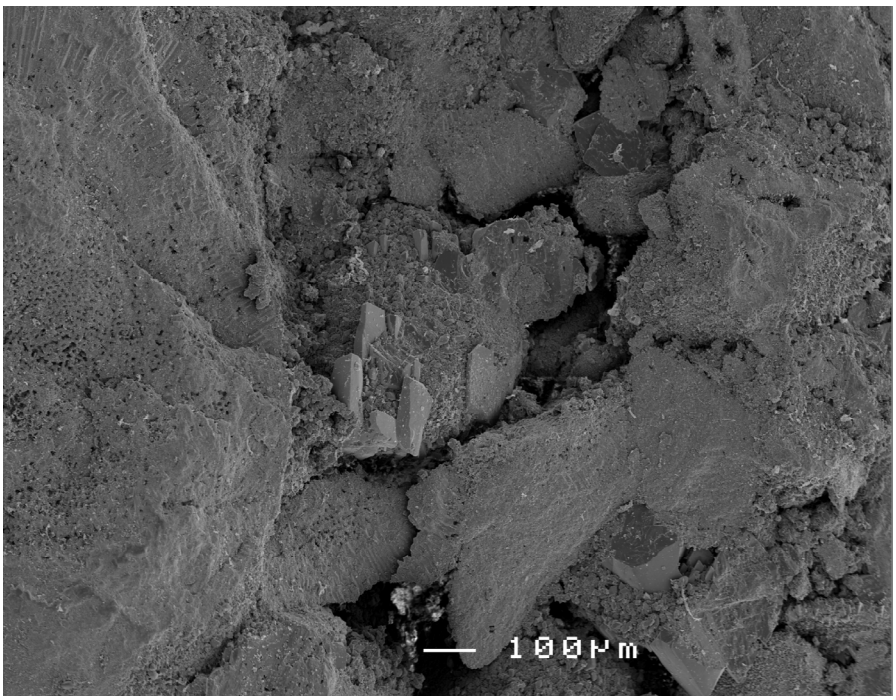


**Host rock cementation**

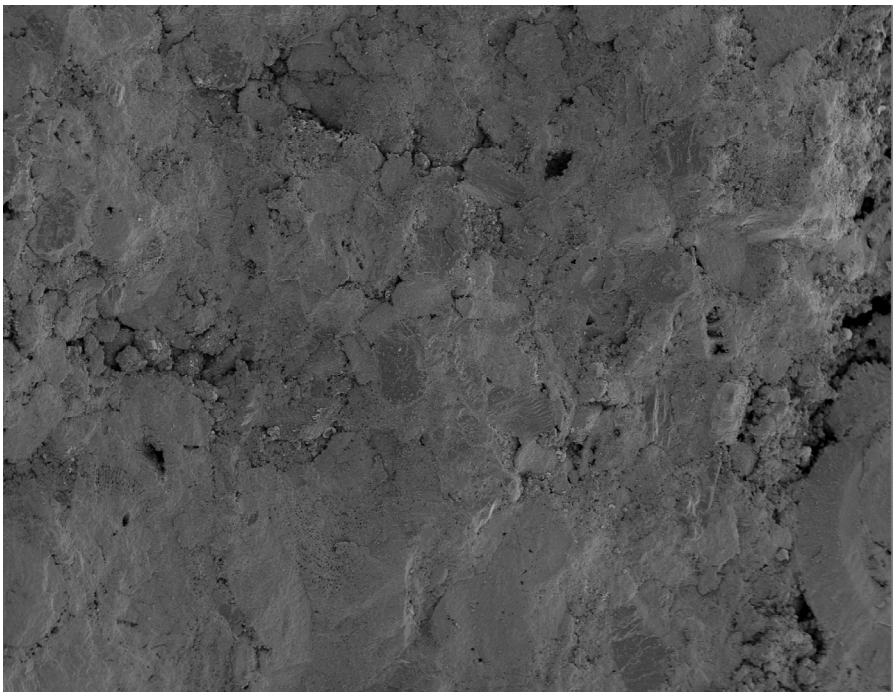

**Inside a deformation band**

## *Electron microprobe*

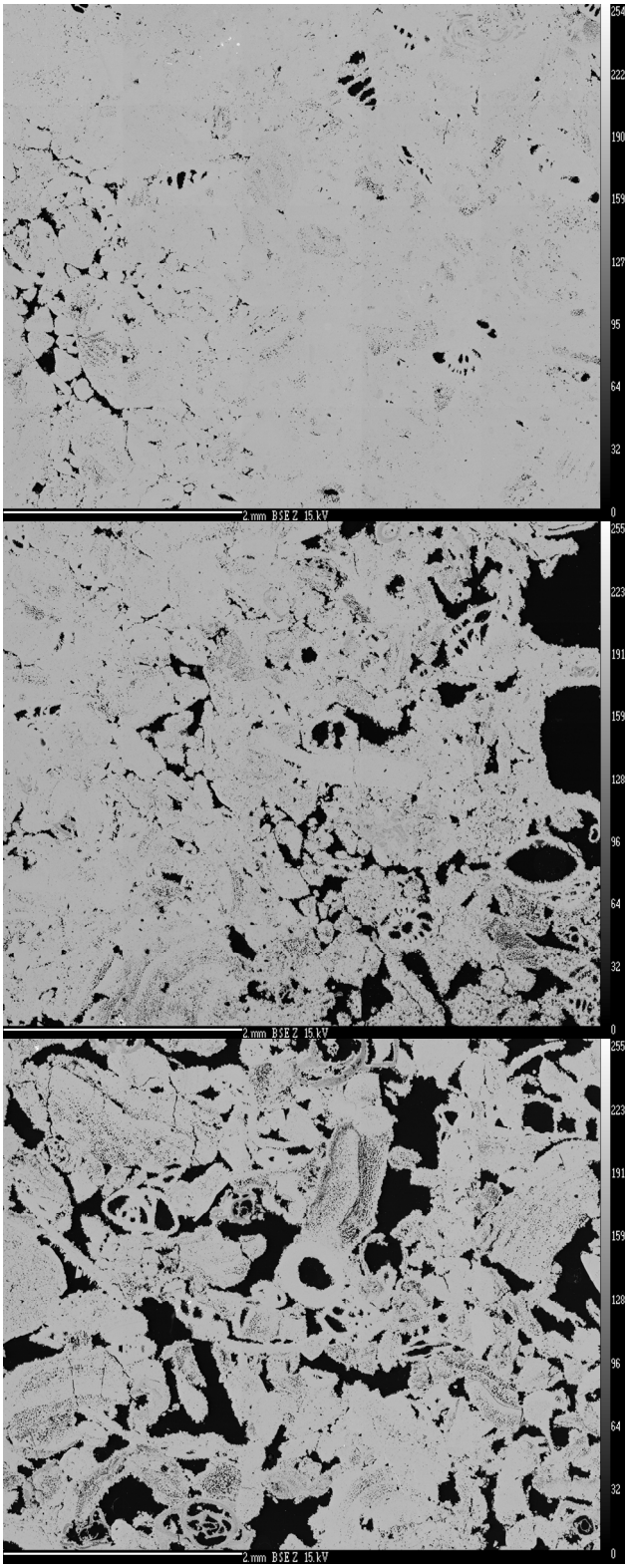


**All images are from the sample Sm1T11n. The first one is shot in the deformation band; the second represents the transition zone between deformation band and host rock; the last is a picture from the non-deformed rock**

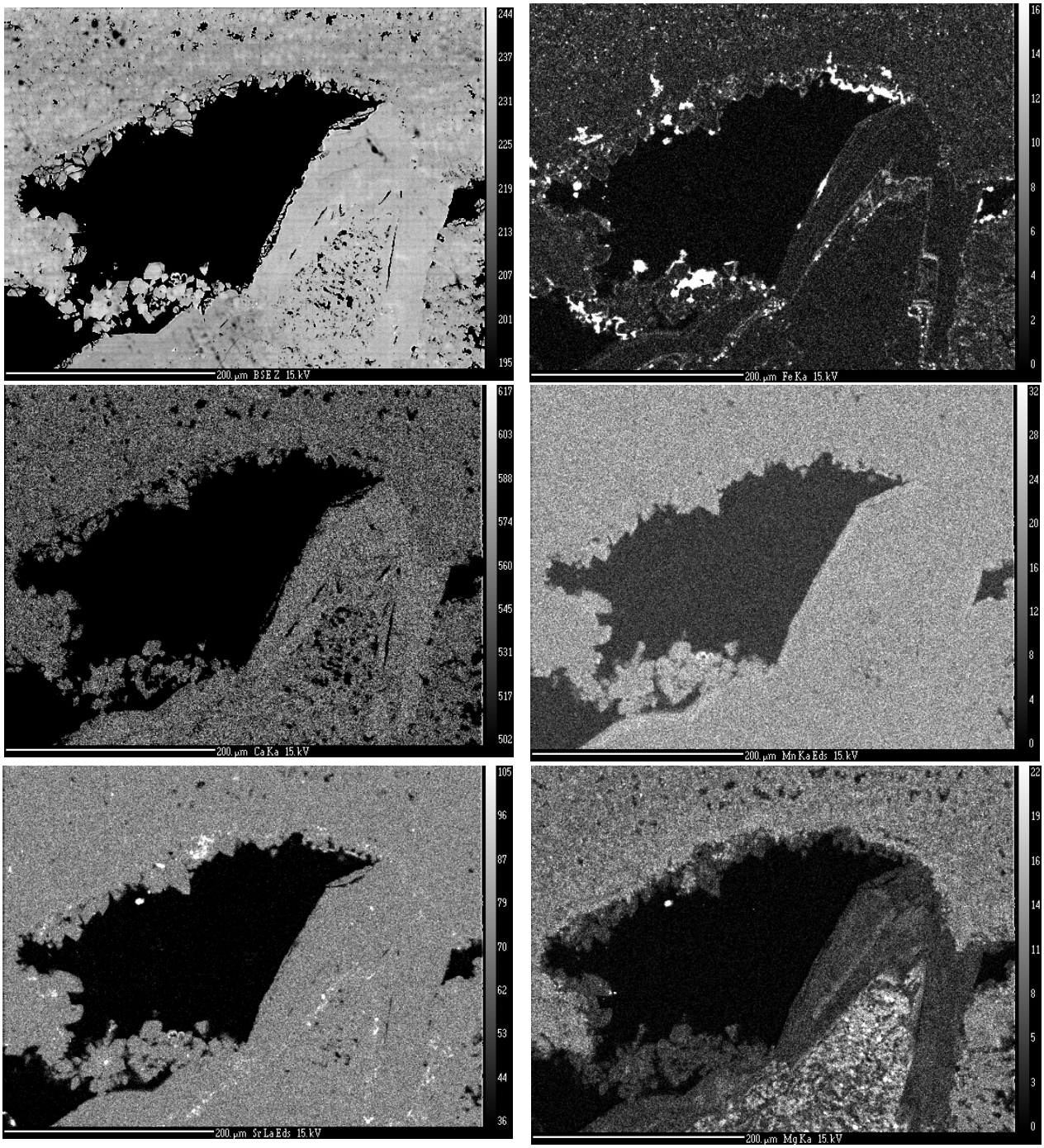


**Element map of a pore in the sample Sm8n, including a BSE image and element maps of the elements Fe, Ca, Mn, Sr, Mg.**

## Results

### *Porosity calculation from thin sections*

Rectangle dimension: 2559/1917 pixels done in a binary calculation

| Thin section | Area | White level | Black level | Porosity |
|---|---|---|---|---|
| Sm9 | **DB** | 4666511 | 239092 | **4,87** |
| Sm9 | *HR* | 3941974 | 963629 | ***19,64*** |
| Sm9 | Trans | 4503686 | 401917 | **8,19** |
| Sm8n | **DB** | 4782017 | 123586 | **2,52** |
| Sm8n | *DB_II* | 4687260 | 218343 | ***4,45*** |
| Sm8n | HR | 3382813 | 1522790 | ***31,04*** |
| Sm8n | Trans | 4183671 | 721932 | **14,72** |
| Sm1T11n | **DB** | 4749612 | 155991 | **3,18** |
| Sm1T11n | *HR* | 3731211 | 1174932 | ***23,95*** |
| Sm1T11n | Trans | 4057067 | 848536 | **17,30** |

### *Permeability of drill cores*

## GAS PERMEABILITY

**SENSOR** **Uni Wien** **Date** **06.06.2008**

**TEMPERATURE OF GAS [°C]** 23,4
**GAS - VISCOSITY [mPas]** **0,0176**

| Drill core # | L [cm] | D [cm] | $P_v$ [bar] | $P_n$ [bar a] | $Q_{Gas}$ [mlN/min] | $k_{Gas}$ [md] |
|---|---|---|---|---|---|---|
| **1** | 7,36 | 2,95 | 0,315 | 0,992 | 4.106 | **4.325,49** |
| **2** | 8,07 | 2,95 | 1,309 | 0,992 | 4.106 | **753,71** |
| **SM1 T22u** | 3,80 | 2,95 | 9,228 | 0,992 | 1.617 | **5,70** |
| **SM9** | 3,96 | 2,95 | 1,596 | 0,992 | 4.106 | **278,06** |
| **SM2 T22M** | 4,08 | 2,95 | 9,300 | 0,992 | 449 | **1,67** |
| **SM1 T11** | 3,77 | 2,96 | 9,145 | 0,992 | 2.409 | **8,51** |
| **SM7** | 3,76 | 2,95 | 2,943 | 0,992 | 4.106 | **103,24** |
| **SM2 T12** | 4,19 | 2,95 | 8,438 | 0,992 | 4.106 | **18,84** |
| **Sm1 T12M a** | 4,72 | 2,95 | 0,132 | 0,998 | 4.106 | **7.976,50** |
| **Sm1 T12M b** | 5,28 | 2,96 | 6,440 | 0,998 | 901 | **8,38** |
| **Sm9 nDB a** | 4,49 | 2,94 | 0,213 | 0,998 | 4.106 | **4.253,09** |
| **Sm9 nDB b** | 5,73 | 2,96 | 2,206 | 0,998 | 4.106 | **246,23** |

## *Amount of cement*

| **Sm9_1** | | **In the deformation band** |
|---|---|---|
| Porosity+Cement | **17,6** | **%** |
| Porosity | **7,3** | **%** |
| Cement | **10,3** | **%** |
| Rock | **82,4** | **%** |

| **Sm9_2** | | **Adjacent to the deformation band** |
|---|---|---|
| Porosity+Cement | **28,8** | **%** |
| Porosity | **14,7** | **%** |
| Cement | **14,1** | **%** |
| Rock | **71,2** | **%** |

| **Sm9_3** | | **Host rock** |
|---|---|---|
| Porosity+Cement | **35,2** | **%** |
| Porosity | **19,5** | **%** |
| Cement | **15,8** | **%** |
| Rock | **64,8** | **%** |

| **Sm8n_Zone 2** | | **In the deformation band** |
|---|---|---|
| Porosity+Cement | **12,8** | **%** |
| Porosity | **3,7** | **%** |
| Cement | **9,1** | **%** |
| Rock | **87,2** | **%** |

| **Sm8n_Zone 1** | | **Adjacent to the deformation band** |
|---|---|---|
| Porosity+Cement | **2,7** | **%** |
| Porosity | **0,4** | **%** |
| Cement | **2,3** | **%** |
| Rock | **97,3** | **%** |

| **Sm8n_Zone 3** | | **Host rock** |
|---|---|---|
| Porosity+Cement | **29,9** | **%** |
| Porosity | **18,1** | **%** |
| Cement | **11,8** | **%** |
| Rock | **70,1** | **%** |

*Heliumporosity*

**Last calibration: 13.02.2008 at 25.0°C**

| **V Sample cell** | **cm³** | **102,71** | **103,08** | **102,64** | **102,90** | **103,10** | **103,20** | **102,67** | **102,73** | **102,79** | **103,18** | **102,65** | **102,97** |
|---|---|---|---|---|---|---|---|---|---|---|---|---|---|
| **V Exp. cell** | **cm³** | **57,30** | **57,49** | **57,74** | **57,49** | **57,32** | **57,36** | **57,02** | **57,70** | **57,36** | **57,55** | **57,73** | **57,54** |
| **□ Hg** | **g/cm³** | **13,54** | **13,54** | **13,54** | **13,54** | **13,54** | **13,54** | **13,54** | **13,54** | **13,54** | **13,54** | **13,54** | **13,54** |
| **Sensor** | **#** | **1** | **2** | **3** | **4** | **5** | **6** | **7** | **8** | **9** | **10** | **11** | **12** |
| **Depth** | **m** | | | | | | | | | | | | |
| **Drill core** | **#** | **1** | **2** | **SM1 T22u** | **SM9** | **SM2 T22M** | **SM1 T11** | **SM7** | **SM2 T12** | **Sm1 T12M a** | **Sm1 T12M b** | **Sm9 nDB a** | **Sm9 nDB b** |
| **Length** | **cm** | 7,36 | 8,07 | 3,80 | 3,96 | 4,08 | 3,77 | 3,76 | 4,19 | 4,72 | 5,28 | 4,49 | 5,73 |
| **Diameter** | **cm** | 2,95 | 2,95 | 2,95 | 2,95 | 2,95 | 2,95 | 2,95 | 2,95 | 2,95 | 2,96 | 2,94 | 2,96 |
| **Net weight** | **g** | 96,644 | 104,684 | 59,032 | 53,762 | 64,450 | 58,174 | 56,576 | 62,461 | 59,499 | 73,966 | 60,954 | 80,485 |
| **Hg-buoyancy** | **g** | 670,6 | 735,3 | 348,8 | 359,6 | 375,3 | 345,3 | 345,5 | 384,2 | 428,1 | 483,1 | 411,4 | 527,9 |
| **Vol** | **cm³** | 49,53 | 54,31 | 25,76 | 26,56 | 27,72 | 25,50 | 25,52 | 28,38 | 31,62 | 35,68 | 30,38 | 38,99 |
| **P1/1** | **bar** | 1,956 | 1,959 | 1,955 | 1,958 | 1,956 | 1,959 | 1,958 | 1,964 | 1,929 | 1,947 | 1,960 | 1,975 |
| **P2/1** | **bar** | 1,055 | 1,036 | 1,141 | 1,158 | 1,136 | 1,152 | 1,154 | 1,140 | 1,128 | 1,107 | 1,140 | 1,107 |
| **P1/2** | **bar** | 1,955 | 1,958 | 1,955 | 1,957 | 1,955 | 1,959 | 1,958 | 1,964 | 1,925 | 1,945 | 1,957 | 1,972 |
| **P2/2** | **bar** | 1,054 | 1,035 | 1,141 | 1,158 | 1,135 | 1,151 | 1,154 | 1,140 | 1,126 | 1,106 | 1,138 | 1,104 |
| **P1/3** | **bar** | 1,955 | 1,958 | 1,955 | 1,957 | 1,955 | 1,957 | 1,956 | 1,963 | 1,925 | 1,943 | 1,957 | 1,973 |
| **P2/3** | **bar** | 1,054 | 1,034 | 1,140 | 1,157 | 1,134 | 1,150 | 1,153 | 1,138 | 1,126 | 1,105 | 1,138 | 1,105 |
| **Matrix-Vol** | **cm³** | 35,66 | 38,62 | 21,72 | 19,70 | 23,79 | 21,43 | 20,75 | 23,02 | 21,97 | 27,32 | 22,42 | 29,70 |
| **Porosity eff.** | **%** | **28,00** | **28,88** | **15,68** | **25,81** | **14,18** | **15,97** | **18,70** | **18,89** | **30,50** | **23,44** | **26,20** | **23,83** |
| **Density** | **g/cm³** | **2,71** | **2,71** | **2,72** | **2,73** | **2,71** | **2,71** | **2,73** | **2,71** | **2,71** | **2,71** | **2,72** | **2,71** |
| **Volume weight** | **g/cm³** | 1,95 | 1,93 | 2,29 | 2,02 | 2,33 | 2,28 | 2,22 | 2,20 | 1,88 | 2,07 | 2,01 | 2,06 |
| **Pv** | **cm³** | **13,87** | **15,68** | **4,04** | **6,86** | **3,93** | **4,07** | **4,77** | **5,36** | **9,65** | **8,36** | **7,96** | **9,29** |
| **Por.-eff. (from geometry)** | | **29,11** | **29,97** | **16,36** | **27,20** | **14,70** | **16,83** | **19,27** | **19,63** | **31,89** | **24,82** | **26,45** | **24,68** |

## *µCT*

### Calibration

Calibration includes both techniques - the thin section porosity and - the drill core porosity

| Thin section | Analysis of thin sections in | Porosity | Average value to work with | | | | Find spot in the µCT | Find spot in Amira with equivalent dataset | | Threshold in Amira | | Deviation | | |
|---|---|---|---|---|---|---|---|---|---|---|---|---|---|---|
| | | | Scan porosity In [%] | Drill core Porosity In [%] | | | µCT | | | Scan | Kern | from drill core --> Scan | from Scan --> drill core | |
| **Sm1** | **Grayscale** | **6,728529681** | **6,8** | **16,0** | | At image | 417 | 693 | | 3050 | 4185 | **16,4** | **6,7** | Short core |
| **Sm1** | **Grayscale** | **6,870399607** | | | | | | | | | | **9,6** | **-9,3** | |
| **Sm1T11** | **Grayscale** | **26,30351779** | **26,3** | **23,4** | | At image | 1438 | 1205 | 1362 | 6475 | 6300 | **23,3** | **26,2** | Long core |
| **Sm1T11** | **Farbig** | **26,30351779** | | | | | | | | | | **-3,0** | **2,8** | |
| **Sm9** | **Grayscale** | **21,66809666** | **21,7** | **23,9** | | At image | | | | 13900 | 15350 | **30,9** | **17,1** | Short core |
| **Sm9** | **Farbig** | **21,708328** | | | | | | | | | | **7,0** | **-6,8** | |

## Sm9

SM9
Porosity calculation
at threshold value: 15350
Dataset: Sm9_KG2.8_bh4.2
from Network
Sm9

| Data field | Dimensions | Pores | Pores | Rock | Rock | Total volume | Total volume | Porosity |
|---|---|---|---|---|---|---|---|---|
| Unit | Pixel x*x*x | in [pixelcounts] | in [mm³] | in [pixelcounts] | in [mm³] | in [pixelcounts] | in [mm³] | in [%] |
| DB2 | 200 | 573922 | 15,495894 | 7481354 | 201,996558 | 8055276 | 217,492452 | **7,1** |
| Def_band | 200 | 822063 | 22,195701 | 7298538 | 197,060526 | 8120601 | 219,256227 | **10,1** |
| TZ | 200 | 2323064 | 62,722728 | 5797537 | 156,533499 | 8120601 | 219,256227 | **28,6** |
| TZ2 | 200 | 2184164 | 58,972428 | 5936437 | 160,283799 | 8120601 | 219,256227 | **26,9** |
| HR | 300 | 6646463 | 179,454501 | 18398604 | 496,762308 | 25045067 | 676,216809 | **26,5** |
| HR2 | 300 | 6711784 | 181,218168 | 16199503 | 437,386581 | 22911287 | 618,604749 | **29,3** |
| HR_weitweg | 200 | 2048161 | 55,300347 | 5942138 | 160,437726 | 7990299 | 215,738073 | **25,6** |
| DB1 | 75 | 9797 | 0,264519 | 429179 | 11,587833 | 438976 | 11,852352 | **2,2** |
| DB2 | 75 | 4287 | 0,115749 | 434689 | 11,736603 | 438976 | 11,852352 | **1,0** |
| DB3 | 75 | 17564 | 0,474228 | 421412 | 11,378124 | 438976 | 11,852352 | **4,0** |
| DB4 | 75 | 22578 | 0,609606 | 416398 | 11,242746 | 438976 | 11,852352 | **5,1** |
| DB5 | 75 | 22736 | 0,613872 | 416240 | 11,23848 | 438976 | 11,852352 | **5,2** |
| DB6 | 75 | 17137 | 0,462699 | 421839 | 11,389653 | 438976 | 11,852352 | **3,9** |
| Profile1 | 75 | 183273 | 4,948371 | 255702 | 6,903954 | 438975 | 11,852325 | **41,8** |
| Profile2 | 75 | 161558 | 4,362066 | 277418 | 7,490286 | 438976 | 11,852352 | **36,8** |
| Profile3 | 75 | 130290 | 3,51783 | 308686 | 8,334522 | 438976 | 11,852352 | **29,7** |
| Profile4 | 75 | 124281 | 3,355587 | 314695 | 8,496765 | 438976 | 11,852352 | **28,3** |
| Profile5 | 75 | 114500 | 3,0915 | 324476 | 8,760852 | 438976 | 11,852352 | **26,1** |
| Profile6 | 75 | 39684 | 1,071468 | 399292 | 10,780884 | 438976 | 11,852352 | **9,0** |
| Profile7 | 75 | 27701 | 0,747927 | 411275 | 11,104425 | 438976 | 11,852352 | **6,3** |
| Profile8 | 75 | 48303 | 1,304181 | 390673 | 10,548171 | 438976 | 11,852352 | **11,0** |
| rofile9 | 75 | 120093 | 3,242511 | 318883 | 8,609841 | 438976 | 11,852352 | **27,4** |

| Data field | Dimensions | Pores | Pores | Rock | Rock | Total volume | Total volume | Porosity |
|---|---|---|---|---|---|---|---|---|
| Unit | Pixel x*x*x | in [pixelcounts] | in [mm³] | in [pixelcounts] | in [mm³] | in [pixelcounts] | in [mm³] | in [%] |
| Profile10 | 75 | 141079 | 3,809133 | 297897 | 8,043219 | 438976 | 11,852352 | **32,1** |
| Profile11 | 75 | 157296 | 4,246992 | 281680 | 7,60536 | 438976 | 11,852352 | **35,8** |
| Profile12 | 75 | 171805 | 4,638735 | 267171 | 7,213617 | 438976 | 11,852352 | **39,1** |
| Profile13 | 75 | 140634 | 3,797118 | 298342 | 8,055234 | 438976 | 11,852352 | **32,0** |
| Profile14 | 75 | 140357 | 3,789639 | 298619 | 8,062713 | 438976 | 11,852352 | **32,0** |
| | | 1050 | | | | | | |

SM9
Porosity calculation
at threshold value: 13900
Dataset: Sm9_KG2.8_bh4.2_test
from Network Sm9_test

| Data field | Dimensions | Pores | Pores | Rock | Rock | Total volume | Total volume | Porosity | Data field | Data field | | | |
|---|---|---|---|---|---|---|---|---|---|---|---|---|---|
| Unit | Pixel x*x*x | in [pixelcounts] | in [mm³] | in [pixelcounts] | in [mm³] | in [pixelcounts] | in [mm³] | in [%] | [z-Axis] | [z-Axis in mm] | | | |
| Sm9_Profile_1 | 101 | 212966 | 5,750082 | 817335 | 22,068045 | 1030301 | 27,818127 | **20,7** | 0-100 | 1,5 | Data range | | |
| Sm9_Profile_2 | 101 | 198973 | 5,372271 | 831328 | 22,445856 | 1030301 | 27,818127 | **19,3** | 100-200 | 4,5 | x | 200 | 300 |
| Sm9_Profile_3 | 101 | 172464 | 4,656528 | 857837 | 23,161599 | 1030301 | 27,818127 | **16,7** | 200-300 | 7,5 | y | 200 | 300 |
| Sm9_Profile_4 | 101 | 163158 | 4,405266 | 867143 | 23,412861 | 1030301 | 27,818127 | **15,8** | 300-400 | 10,5 | z | 0 | 1100 |
| Sm9_Profile_5 | 101 | 107317 | 2,897559 | 922984 | 24,920568 | 1030301 | 27,818127 | **10,4** | 400-500 | 13,5 | | | |
| Sm9_Profile_6 | 101 | 21050 | 0,56835 | 1009251 | 27,249777 | 1030301 | 27,818127 | **2,0** | 500-600 | 16,5 | | | |
| Sm9_Profile_7 | 101 | 71318 | 1,925586 | 958983 | 25,892541 | 1030301 | 27,818127 | **6,9** | 600-700 | 19,5 | | | |
| Sm9_Profile_8 | 101 | 242132 | 6,537564 | 788169 | 21,280563 | 1030301 | 27,818127 | **23,5** | 700-800 | 22,5 | | | |
| Sm9_Profile_9 | 101 | 188538 | 5,090526 | 841763 | 22,727601 | 1030301 | 27,818127 | **18,3** | 800-900 | 25,5 | | | |
| Sm9_Profile_10 | 101 | 255966 | 6,911082 | 774335 | 20,907045 | 1030301 | 27,818127 | **24,8** | 900-1000 | 28,5 | | | |
| Sm9_Profile_11 | 101 | 188761 | 5,096547 | 841540 | 22,72158 | 1030301 | 27,818127 | **18,3** | 1000-1100 | 31,5 | | | |
| | | | | | | | | | | | | | |
| Sm9_Profile2_1 | 101 | 192080 | 5,18616 | 838221 | 22,631967 | 1030301 | 27,818127 | **18,6** | 0-100 | 1,5 | Data range | | |
| Sm9_Profile2_2 | 101 | 175900 | 4,7493 | 854401 | 23,068827 | 1030301 | 27,818127 | **17,1** | 100-200 | 4,5 | x | 600 | 700 |
| Sm9_Profile2_3 | 101 | 185762 | 5,015574 | 844539 | 22,802553 | 1030301 | 27,818127 | **18,0** | 200-300 | 7,5 | y | 200 | 300 |
| Sm9_Profile2_4 | 101 | 188756 | 5,096412 | 841545 | 22,721715 | 1030301 | 27,818127 | **18,3** | 300-400 | 10,5 | z | 0 | 1100 |
| Sm9_Profile2_5 | 101 | 172235 | 4,650345 | 858066 | 23,167782 | 1030301 | 27,818127 | **16,7** | 400-500 | 13,5 | | | |

| Data field | Dimensions | Pores | Pores | Rock | Rock | Total volume | Total volume | Porosity | Data field | Data field |
|---|---|---|---|---|---|---|---|---|---|---|
| Unit | Pixel x*x*x | in [pixelcounts] | in [mm³] | in [pixelcounts] | in [mm³] | in [pixelcounts] | in [mm³] | in [%] | [z-Axis] | [z-Axis in mm] |
| Sm9_Profile2_6 | 101 | 42412 | 1,145124 | 987889 | 26,673003 | 1030301 | 27,818127 | **4,1** | 500-600 | 16,5 |
| Sm9_Profile2_7 | 101 | 33859 | 0,914193 | 996442 | 26,903934 | 1030301 | 27,818127 | **3,3** | 600-700 | 19,5 |
| Sm9_Profile2_8 | 101 | 109509 | 2,956743 | 920792 | 24,861384 | 1030301 | 27,818127 | **10,6** | 700-800 | 22,5 |
| Sm9_Profile2_9 | 101 | 213203 | 5,756481 | 817098 | 22,061646 | 1030301 | 27,818127 | **20,7** | 800-900 | 25,5 |
| Sm9_Profile2_10 | 101 | 229998 | 6,209946 | 800303 | 21,608181 | 1030301 | 27,818127 | **22,3** | 900-1000 | 28,5 |
| Sm9_Profile2_11 | 101 | 190060 | 5,13162 | 840241 | 22,686507 | 1030301 | 27,818127 | **18,4** | 1000-1100 | 31,5 |
| | | | | | | | | | | |
| Sm9_Profile3_1 | 101 | 196402 | 5,302854 | 833899 | 22,515273 | 1030301 | 27,818127 | **19,1** | 0-100 | 1,5 |
| Sm9_Profile3_2 | 101 | 175385 | 4,735395 | 854916 | 23,082732 | 1030301 | 27,818127 | **17,0** | 100-200 | 4,5 |
| Sm9_Profile3_3 | 101 | 193464 | 5,223528 | 836837 | 22,594599 | 1030301 | 27,818127 | **18,8** | 200-300 | 7,5 |
| Sm9_Profile3_4 | 101 | 160167 | 4,324509 | 870134 | 23,493618 | 1030301 | 27,818127 | **15,5** | 300-400 | 10,5 |
| Sm9_Profile3_5 | 101 | 28138 | 0,759726 | 1002163 | 27,058401 | 1030301 | 27,818127 | **2,7** | 400-500 | 13,5 |
| Sm9_Profile3_6 | 101 | 46038 | 1,243026 | 984263 | 26,575101 | 1030301 | 27,818127 | **4,5** | 500-600 | 16,5 |
| Sm9_Profile3_7 | 101 | 202452 | 5,466204 | 827849 | 22,351923 | 1030301 | 27,818127 | **19,6** | 600-700 | 19,5 |
| Sm9_Profile3_8 | 101 | 191748 | 5,177196 | 838553 | 22,640931 | 1030301 | 27,818127 | **18,6** | 700-800 | 22,5 |
| Sm9_Profile3_9 | 101 | 146838 | 3,964626 | 883463 | 23,853501 | 1030301 | 27,818127 | **14,3** | 800-900 | 25,5 |
| Sm9_Profile3_10 | 101 | 164069 | 4,429863 | 866232 | 23,388264 | 1030301 | 27,818127 | **15,9** | 900-1000 | 28,5 |
| Sm9_Profile3_11 | 101 | 178088 | 4,808376 | 852213 | 23,009751 | 1030301 | 27,818127 | **17,3** | 1000-1100 | 31,5 |
| | | | | | | | | | | |
| Sm9_Profile4_1 | 101 | 195984 | 5,291568 | 834317 | 22,526559 | 1030301 | 27,818127 | **19,0** | 0-100 | 1,5 |
| Sm9_Profile4_2 | 101 | 179154 | 4,837158 | 851147 | 22,980969 | 1030301 | 27,818127 | **17,4** | 100-200 | 4,5 |
| Sm9_Profile4_3 | 101 | 233026 | 6,291702 | 797275 | 21,526425 | 1030301 | 27,818127 | **22,6** | 200-300 | 7,5 |
| Sm9_Profile4_4 | 101 | 210200 | 5,6754 | 820101 | 22,142727 | 1030301 | 27,818127 | **20,4** | 300-400 | 10,5 |
| Sm9_Profile4_5 | 101 | 119721 | 3,232467 | 910580 | 24,58566 | 1030301 | 27,818127 | **11,6** | 400-500 | 13,5 |
| Sm9_Profile4_6 | 101 | 51922 | 1,401894 | 978379 | 26,416233 | 1030301 | 27,818127 | **5,0** | 500-600 | 16,5 |
| Sm9_Profile4_7 | 101 | 29475 | 0,795825 | 1000826 | 27,022302 | 1030301 | 27,818127 | **2,9** | 600-700 | 19,5 |
| Sm9_Profile4_8 | 101 | 153433 | 4,142691 | 876868 | 23,675436 | 1030301 | 27,818127 | **14,9** | 700-800 | 22,5 |
| Sm9_Profile4_9 | 101 | 171626 | 4,633902 | 858675 | 23,184225 | 1030301 | 27,818127 | **16,7** | 800-900 | 25,5 |
| Sm9_Profile4_10 | 101 | 228235 | 6,162345 | 802066 | 21,655782 | 1030301 | 27,818127 | **22,2** | 900-1000 | 28,5 |
| Sm9_Profile4_11 | 101 | 174293 | 4,705911 | 856008 | 23,112216 | 1030301 | 27,818127 | **16,9** | 1000-1100 | 31,5 |

| Data range | | |
|---|---|---|
| x | 200 | 300 |
| y | 600 | 700 |
| z | 0 | 1100 |

| Data range | | |
|---|---|---|
| x | 600 | 700 |
| y | 600 | 700 |
| z | 0 | 1100 |

| Data field | Dimensions | Pores | Pores | Rock | Rock | Total volume | Total volume | Porosity | Data field | Data field | | | |
|---|---|---|---|---|---|---|---|---|---|---|---|---|---|
| Unit | Pixel x*x*x | in [pixelcounts] | in [mm³] | in [pixelcounts] | in [mm³] | in [pixelcounts] | in [mm³] | in [%] | [z-Axis] | [z-Axis in mm] | | | |
| Sm9_Profile5_1 | 101 | 232038 | 6,265026 | 798263 | 21,553101 | 1030301 | 27,81827 | **22,5** | 0-100 | 1,5 | | Data range | |
| Sm9_Profile5_2 | 101 | 262777 | 7,094979 | 767524 | 20,723148 | 1030301 | 27,818127 | **25,5** | 100-200 | 4,5 | x | 416 | 516 |
| Sm9_Profile5_3 | 101 | 221681 | 5,985387 | 808620 | 21,83274 | 1030301 | 27,818127 | **21,5** | 200-300 | 7,5 | y | 416 | 516 |
| Sm9_Profile5_4 | 101 | 212079 | 5,726133 | 818222 | 22,091994 | 1030301 | 27,818127 | **20,6** | 300-400 | 10,5 | z | 0 | 1100 |
| Sm9_Profile5_5 | 101 | 163363 | 4,410801 | 866938 | 23,407326 | 1030301 | 27,818127 | **15,9** | 400-500 | 13,5 | | | |
| Sm9_Profile5_6 | 101 | 21414 | 0,578178 | 1008887 | 27,239949 | 1030301 | 27,818127 | **2,1** | 500-600 | 16,5 | | | |
| Sm9_Profile5_7 | 101 | 137246 | 3,705642 | 893055 | 24,112485 | 1030301 | 27,818127 | **13,3** | 600-700 | 19,5 | | | |
| Sm9_Profile5_8 | 101 | 238617 | 6,442659 | 791684 | 21,375468 | 1030301 | 27,818127 | **23,2** | 700-800 | 22,5 | | | |
| Sm9_Profile5_9 | 101 | 217427 | 5,870529 | 812874 | 21,947598 | 1030301 | 27,818127 | **21,1** | 800-900 | 25,5 | | | |
| Sm9_Profile5_10 | 101 | 223695 | 6,039765 | 806606 | 21,778362 | 1030301 | 27,818127 | **21,7** | 900-1000 | 28,5 | | | |
| Sm9_Profile5_11 | 101 | 278756 | 7,526412 | 751545 | 20,291715 | 1030301 | 27,818127 | **27,1** | 1000-1100 | 31,5 | | | |

| | Porosity in [log] |
|---|---|
| **Average [log]** | **1,30068** |
| | **1,28466** |
| | **1,290835** |
| | **1,25858** |
| | **1,059487** |
| | **0,550128** |
| | **0,964165** |
| | **1,259081** |
| | **1,260098** |
| | **1,330233** |
| | **1,292369** |

| | Porosity in [%] | | |
|---|---|---|---|
| **Average** | **20,0** | 0-100 | 1,5 |
| | **19,3** | 100-200 | 4,5 |
| | **19,5** | 200-300 | 7,5 |
| | **18,1** | 300-400 | 10,5 |
| | **11,5** | 400-500 | 13,5 |
| | **3,5** | 500-600 | 16,5 |
| | **9,2** | 600-700 | 19,5 |
| | **18,2** | 700-800 | 22,5 |
| | **18,2** | 800-900 | 25,5 |
| | **21,4** | 900-1000 | 28,5 |
| | **19,6** | 1000-1100 | 31,5 |

## Sm1

SM1
Porosity calculation
at threshold value: 3050
Dataset:Sm1_Arbeitsmaterial
from Network Sm1

| Data field<br>Unit | Dimensions<br>Pixel x*x*x | Pores<br>in [pixelcounts] | Pores<br>in [mm³] | Rock<br>in [pixelcounts] | Rock<br>in [mm³] | Total volume<br>in [pixelcounts] | Total volume<br>in [mm³] | Porosity<br>in [%] |
|---|---|---|---|---|---|---|---|---|
| Sm1_1 | 76 | 22490 | 0,60723 | 56398 | 1,522746 | 78888 | 2,129976 | **28,5** |
| Sm1_2 | 76 | 66245 | 1,788615 | 301443 | 8,138961 | 367688 | 9,927576 | **18,0** |
| Sm1_3 | 76 | 71999 | 1,943973 | 366977 | 9,908379 | 438976 | 11,852352 | **16,4** |
| Sm1_4 | 76 | 76113 | 2,055051 | 362863 | 9,797301 | 438976 | 11,852352 | **17,3** |
| Sm1_5 | 76 | 50632 | 1,367064 | 388344 | 10,485288 | 438976 | 11,852352 | **11,5** |
| Sm1_6 | 76 | 8957 | 0,241839 | 430019 | 11,610513 | 438976 | 11,852352 | **2,0** |
| Sm1_7 | 76 | 10265 | 0,277155 | 428711 | 11,575197 | 438976 | 11,852352 | **2,3** |
| Sm1_8 | 76 | 5331 | 0,143937 | 433645 | 11,708415 | 438976 | 11,852352 | **1,2** |
| Sm1_9 | 76 | 2003 | 0,054081 | 436973 | 11,798271 | 438976 | 11,852352 | **0,5** |
| Sm1_10 | 76 | 2710 | 0,07317 | 436266 | 11,779182 | 438976 | 11,852352 | **0,6** |
| Sm1_11 | 76 | 1831 | 0,049437 | 437145 | 11,802915 | 438976 | 11,852352 | **0,4** |
| Sm1_12 | 76 | 14717 | 0,397359 | 424259 | 11,454993 | 438976 | 11,852352 | **3,4** |
| Sm1_13 | 76 | 25250 | 0,68175 | 413726 | 11,170602 | 438976 | 11,852352 | **5,8** |
| Sm1_DB_1 | 76 | 3497 | 0,094419 | 435479 | 11,757933 | 438976 | 11,852352 | **0,8** |
| Sm1_DB_2 | 76 | 3399 | 0,091773 | 435577 | 11,760579 | 438976 | 11,852352 | **0,8** |
| Sm1_DB_3 | 76 | 3913 | 0,105651 | 435063 | 11,746701 | 438976 | 11,852352 | **0,9** |
| Sm1_DB_4 | 76 | 1460 | 0,03942 | 437516 | 11,812932 | 438976 | 11,852352 | **0,3** |
| Sm1_DB_5 | 76 | 5468 | 0,147636 | 433508 | 11,704716 | 438976 | 11,852352 | **1,2** |
| Sm1_DB_6 | 76 | 8238 | 0,222426 | 430738 | 11,629926 | 438976 | 11,852352 | **1,9** |
| Sm1_DB_7 | 76 | 2593 | 0,070011 | 436383 | 11,782341 | 438976 | 11,852352 | **0,6** |
| Sm1_DB_8 | 76 | 3471 | 0,093717 | 435505 | 11,758635 | 438976 | 11,852352 | **0,8** |
| Sm1_DB_9 | 76 | 2445 | 0,066015 | 436531 | 11,786337 | 438976 | 11,852352 | **0,6** |
| Sm1_DB_10 | 76 | 2248 | 0,060696 | 436728 | 11,791656 | 438976 | 11,852352 | **0,5** |

| Data field<br>Unit | Dimensions<br>Pixel x*x*x | Pores<br>in [pixelcounts] | Pores<br>in [mm³] | Rock<br>in [pixelcounts] | Rock<br>in [mm³] | Total volume<br>in [pixelcounts] | Total volume<br>in [mm³] | Porosity<br>in [%] |
|---|---|---|---|---|---|---|---|---|
| Sm1_DB_11 | 76 | 5689 | 0,153603 | 433287 | 11,698749 | 438976 | 11,852352 | **1,3** |
| Sm1_DB_12 | 76 | 8590 | 0,23193 | 430386 | 11,620422 | 438976 | 11,852352 | **2,0** |
| Sm1_HR_1 | 201 | 1473957 | 39,796839 | 6383133 | 172,344591 | 7857090 | 212,14143 | **18,8** |
| Sm1_HR_2 | 201 | 1243768 | 33,581736 | 4527746 | 122,249142 | 5771514 | 155,830878 | **21,6** |
| Sm1_Profile1 | 76 | 27531 | 0,743337 | 411445 | 11,109015 | 438976 | 11,852352 | **6,3** |
| Sm1_Profile2 | 76 | 41444 | 1,118988 | 397532 | 10,733364 | 438976 | 11,852352 | **9,4** |
| Sm1_Profile3 | 76 | 15599 | 0,421173 | 423377 | 11,431179 | 438976 | 11,852352 | **3,6** |
| Sm1_Profile4 | 76 | 5336 | 0,144072 | 433640 | 11,70828 | 438976 | 11,852352 | **1,2** |
| Sm1_Profile5 | 76 | 6606 | 0,178362 | 432370 | 11,67399 | 438976 | 11,852352 | **1,5** |
| Sm1_Profile6 | 76 | 2882 | 0,077814 | 436094 | 11,774538 | 438976 | 11,852352 | **0,7** |
| Sm1_Profile7 | 76 | 25260 | 0,68202 | 413716 | 11,170332 | 438976 | 11,852352 | **5,8** |
| Sm1_Profile8 | 76 | 58830 | 1,58841 | 380146 | 10,263942 | 438976 | 11,852352 | **13,4** |
| Sm1_Profile9 | 76 | 71404 | 1,927908 | 367572 | 9,924444 | 438976 | 11,852352 | **16,3** |
| Sm1_Profile10 | 76 | 74953 | 2,023731 | 364023 | 9,828621 | 438976 | 11,852352 | **17,1** |
| Sm1_Profile11 | 76 | 73363 | 1,980801 | 365613 | 9,871551 | 438976 | 11,852352 | **16,7** |
| Sm1_DB-F_1 | 76 | 7561 | 0,204147 | 431415 | 11,648205 | 438976 | 11,852352 | **1,7** |
| Sm1_DB-F_2 | 76 | 4873 | 0,131571 | 434103 | 11,720781 | 438976 | 11,852352 | **1,1** |
| Sm1_DB-F_3 | 76 | 3804 | 0,102708 | 435172 | 11,749644 | 438976 | 11,852352 | **0,9** |
| Sm1_DB-F_4 | 76 | 5582 | 0,150714 | 433394 | 11,701638 | 438976 | 11,852352 | **1,3** |

## Sm1T11

SM1T11
Porosity calculation
at threshold value: 6475
Dataset: Sm1T11 Arbeitsmaterial_neu
from Network Sm1T11_richtiger Datensatz

| Data field<br>Unit | Dim. Pixel<br>x*x*x | Pores in<br>[pixelcounts] | Pores<br>in [mm³] | Rock in<br>[pixelcounts] | Rock<br>in [mm³] | Total volume<br>in [pixelcounts] | Total volume<br>in [mm³] | Porosity<br>in [%] | Data field<br>[z-Axis] | D. f. [z-in mm] | |
|---|---|---|---|---|---|---|---|---|---|---|---|
| Sm1_T11_profile_1 | 101 | 387065 | 24,77216 | 643236 | 41,167104 | 1030301 | 65,939264 | **37,6** | 100-200 | 6,0 | Data range |
| Sm1_T11_profile_2 | 101 | 248665 | 15,91456 | 781636 | 50,024704 | 1030301 | 65,939264 | **24,1** | 200-300 | 10,0 | x 100 200 |
| Sm1_T11_profile_3 | 101 | 272351 | 17,430464 | 757950 | 48,5088 | 1030301 | 65,939264 | **26,4** | 300-400 | 14,0 | y 100 200 |
| Sm1_T11_profile_4 | 101 | 181922 | 11,643008 | 848379 | 54,296256 | 1030301 | 65,939264 | **17,7** | 400-500 | 18,0 | z 100-2200 |
| Sm1_T11_profile_5 | 101 | 154150 | 9,8656 | 876151 | 56,073664 | 1030301 | 65,939264 | **15,0** | 500-600 | 22,0 | |
| Sm1_T11_profile_6 | 101 | 112250 | 7,184 | 918051 | 58,755264 | 1030301 | 65,939264 | **10,9** | 600-700 | 26,0 | |
| Sm1_T11_profile_7 | 101 | 26171 | 1,674944 | 1004130 | 64,26432 | 1030301 | 65,939264 | **2,5** | 700-800 | 30,0 | |
| Sm1_T11_profile_8 | 101 | 11127 | 0,712128 | 1019174 | 65,227136 | 1030301 | 65,939264 | **1,1** | 800-900 | 34,0 | |
| Sm1_T11_profile_9 | 101 | 111113 | 7,111232 | 919788 | 58,866432 | 1030901 | 65,977664 | **10,8** | 900-1000 | 38,0 | |
| Sm1_T11_profile_10 | 101 | 174253 | 11,152192 | 856048 | 54,787072 | 1030301 | 65,939264 | **16,9** | 1000-1100 | 42,0 | |
| Sm1_T11_profile_11 | 101 | 240004 | 15,360256 | 790297 | 50,579008 | 1030301 | 65,939264 | **23,3** | 1100-1200 | 46,0 | |
| Sm1_T11_profile_12 | 101 | 260649 | 16,681536 | 769652 | 49,257728 | 1030301 | 65,939264 | **25,3** | 1200-1300 | 50,0 | |
| Sm1_T11_profile_13 | 101 | 202805 | 12,97952 | 827496 | 52,959744 | 1030301 | 65,939264 | **19,7** | 1300-1400 | 54,0 | |
| Sm1_T11_profile_14 | 101 | 241197 | 15,436608 | 789104 | 50,502656 | 1030301 | 65,939264 | **23,4** | 1400-1500 | 58,0 | |
| Sm1_T11_profile_15 | 101 | 271525 | 17,3776 | 758776 | 48,561664 | 1030301 | 65,939264 | **26,4** | 1500-1600 | 62,0 | |
| Sm1_T11_profile_16 | 101 | 334814 | 21,428096 | 695487 | 44,511168 | 1030301 | 65,939264 | **32,5** | 1600-1700 | 66,0 | |
| Sm1_T11_profile_17 | 101 | 319310 | 20,43584 | 710991 | 45,503424 | 1030301 | 65,939264 | **31,0** | 1700-1800 | 70,0 | |
| Sm1_T11_profile_18 | 101 | 289087 | 18,501568 | 741214 | 47,437696 | 1030301 | 65,939264 | **28,1** | 1800-1900 | 74,0 | |
| Sm1_T11_profile_19 | 101 | 287202 | 18,380928 | 743099 | 47,558336 | 1030301 | 65,939264 | **27,9** | 1900-2000 | 78,0 | |
| Sm1_T11_profile_20 | 101 | 314958 | 20,157312 | 715343 | 45,781952 | 1030301 | 65,939264 | **30,6** | 2100-2200 | 82,0 | |
| Sm1_T11_profile_21 | 101 | 316982 | 20,286848 | 713319 | 45,652416 | 1030301 | 65,939264 | **30,8** | 2200-2300 | 86,0 | |

| Data field<br>Unit | Dim. Pixel<br>x*x*x | Pores in<br>[pixelcounts] | Pores<br>in [mm³] | Rock in<br>[pixelcounts] | Rock<br>in [mm³] | Total volume<br>in [pixelcounts] | Total volume<br>in [mm³] | Porosity<br>in [%] | Data field<br>[z-Axis] | D. f. [z-in mm] | | |
|---|---|---|---|---|---|---|---|---|---|---|---|---|
| Sm1_T11_profile2_1 | 101 | 315699 | 20,204736 | 714602 | 45,734528 | 1030301 | 65,939264 | **30,6** | 200-300 | 10,0 | Data range | |
| Sm1_T11_profile2_2 | 101 | 275423 | 17,627072 | 754878 | 48,312192 | 1030301 | 65,939264 | **26,7** | 300-400 | 14,0 | x | 450 550 |
| Sm1_T11_profile2_3 | 101 | 254891 | 16,313024 | 775410 | 49,62624 | 1030301 | 65,939264 | **24,7** | 400-500 | 18,0 | y | 400 500 |
| Sm1_T11_profile2_4 | 101 | 144680 | 9,25952 | 885621 | 56,679744 | 1030301 | 65,939264 | **14,0** | 500-600 | 22,0 | z | 200-2200 |
| Sm1_T11_profile2_5 | 101 | 134300 | 8,5952 | 896001 | 57,344064 | 1030301 | 65,939264 | **13,0** | 600-700 | 26,0 | | |
| Sm1_T11_profile2_6 | 101 | 10559 | 0,675776 | 1019742 | 65,263488 | 1030301 | 65,939264 | **1,0** | 700-800 | 30,0 | | |
| Sm1_T11_profile2_7 | 101 | 10725 | 0,6864 | 1019576 | 65,252864 | 1030301 | 65,939264 | **1,0** | 800-900 | 34,0 | | |
| Sm1_T11_profile2_8 | 101 | 41094 | 2,630016 | 989207 | 63,309248 | 1030301 | 65,939264 | **4,0** | 900-1000 | 38,0 | | |
| Sm1_T11_profile2_9 | 101 | 168253 | 10,768192 | 862048 | 55,171072 | 1030301 | 65,939264 | **16,3** | 1000-1100 | 42,0 | | |
| Sm1_T11_profile2_10 | 101 | 120402 | 7,705728 | 909899 | 58,233536 | 1030301 | 65,939264 | **11,7** | 1100-1200 | 46,0 | | |
| Sm1_T11_profile2_11 | 101 | 138685 | 8,87584 | 891616 | 57,063424 | 1030301 | 65,939264 | **13,5** | 1200-1300 | 50,0 | | |
| Sm1_T11_profile2_12 | 101 | 224525 | 14,3696 | 805776 | 51,569664 | 1030301 | 65,939264 | **21,8** | 1300-1400 | 54,0 | | |
| Sm1_T11_profile2_13 | 101 | 239007 | 15,296448 | 791294 | 50,642816 | 1030301 | 65,939264 | **23,2** | 1400-1500 | 58,0 | | |
| Sm1_T11_profile2_14 | 101 | 243802 | 15,603328 | 786499 | 50,335936 | 1030301 | 65,939264 | **23,7** | 1500-1600 | 62,0 | | |
| Sm1_T11_profile2_15 | 101 | 284090 | 18,18176 | 746211 | 47,757504 | 1030301 | 65,939264 | **27,6** | 1600-1700 | 66,0 | | |
| Sm1_T11_profile2_16 | 101 | 281782 | 18,034048 | 748519 | 47,905216 | 1030301 | 65,939264 | **27,3** | 1700-1800 | 70,0 | | |
| Sm1_T11_profile2_17 | 101 | 320247 | 20,495808 | 710054 | 45,443456 | 1030301 | 65,939264 | **31,1** | 1800-1900 | 74,0 | | |
| Sm1_T11_profile2_18 | 101 | 353753 | 22,640192 | 676548 | 43,299072 | 1030301 | 65,939264 | **34,3** | 1900-2000 | 78,0 | | |
| Sm1_T11_profile2_19 | 101 | 286697 | 18,348608 | 743604 | 47,590656 | 1030301 | 65,939264 | **27,8** | 2100-2200 | 82,0 | | |
| Sm1_T11_profile2_20 | 101 | 365523 | 23,393472 | 664778 | 42,545792 | 1030301 | 65,939264 | **35,5** | 2200-2300 | 86,0 | | |
| | | | | | | | | | | | | |
| Sm1_T11_profile3_1 | 101 | 317716 | 20,333824 | 712585 | 45,60544 | 1030301 | 65,939264 | **30,8** | 200-300 | 10,0 | Data range | |
| Sm1_T11_profile3_2 | 101 | 306889 | 19,640896 | 723412 | 46,298368 | 1030301 | 65,939264 | **29,8** | 300-400 | 14,0 | x | 400 500 |
| Sm1_T11_profile3_3 | 101 | 248348 | 15,894272 | 781953 | 50,044992 | 1030301 | 65,939264 | **24,1** | 400-500 | 18,0 | y | 100 200 |
| Sm1_T11_profile3_4 | 101 | 220045 | 14,08288 | 810256 | 51,856384 | 1030301 | 65,939264 | **21,4** | 500-600 | 22,0 | z | 200-2200 |
| Sm1_T11_profile3_5 | 101 | 85651 | 5,481664 | 944650 | 60,4576 | 1030301 | 65,939264 | **8,3** | 600-700 | 26,0 | | |
| Sm1_T11_profile3_6 | 101 | 31705 | 2,02912 | 998596 | 63,910144 | 1030301 | 65,939264 | **3,1** | 700-800 | 30,0 | | |
| Sm1_T11_profile3_7 | 101 | 12506 | 0,800384 | 1017795 | 65,13888 | 1030301 | 65,939264 | **1,2** | 800-900 | 34,0 | | |
| Sm1_T11_profile3_8 | 101 | 27019 | 1,729216 | 1003282 | 64,210048 | 1030301 | 65,939264 | **2,6** | 900-1000 | 38,0 | | |
| Sm1_T11_profile3_9 | 101 | 107144 | 6,857216 | 923157 | 59,082048 | 1030301 | 65,939264 | **10,4** | 1000-1100 | 42,0 | | |
| Sm1_T11_profile3_10 | 101 | 105875 | 6,776 | 924426 | 59,163264 | 1030301 | 65,939264 | **10,3** | 1100-1200 | 46,0 | | |

| Data field<br>Unit | Dim. Pixel<br>x*x*x | Pores in<br>[pixelcounts] | Pores<br>in [mm³] | Rock in<br>[pixelcounts] | Rock<br>in [mm³] | Total volume<br>in [pixelcounts] | Total volume<br>in [mm³] | Porosity<br>in [%] | Data field<br>[z-Axis] | D. f. [z-in mm] |
|---|---|---|---|---|---|---|---|---|---|---|
| Sm1_T11_profile3_11 | 101 | 155178 | 9,931392 | 875123 | 56,007872 | 1030301 | 65,939264 | **15,1** | 1200-1300 | 50,0 |
| Sm1_T11_profile3_12 | 101 | 213596 | 13,670144 | 816705 | 52,26912 | 1030301 | 65,939264 | **20,7** | 1300-1400 | 54,0 |
| Sm1_T11_profile3_13 | 101 | 273645 | 17,51328 | 756656 | 48,425984 | 1030301 | 65,939264 | **26,6** | 1400-1500 | 58,0 |
| Sm1_T11_profile3_14 | 101 | 316990 | 20,28736 | 713311 | 45,651904 | 1030301 | 65,939264 | **30,8** | 1500-1600 | 62,0 |
| Sm1_T11_profile3_15 | 101 | 313137 | 20,040768 | 717164 | 45,898496 | 1030301 | 65,939264 | **30,4** | 1600-1700 | 66,0 |
| Sm1_T11_profile3_16 | 101 | 277529 | 17,761856 | 752772 | 48,177408 | 1030301 | 65,939264 | **26,9** | 1700-1800 | 70,0 |
| Sm1_T11_profile3_17 | 101 | 337119 | 21,575616 | 693182 | 44,363648 | 1030301 | 65,939264 | **32,7** | 1800-1900 | 74,0 |
| Sm1_T11_profile3_18 | 101 | 326476 | 20,894464 | 703825 | 45,0448 | 1030301 | 65,939264 | **31,7** | 1900-2000 | 78,0 |
| Sm1_T11_profile3_19 | 101 | 272633 | 17,448512 | 757668 | 48,490752 | 1030301 | 65,939264 | **26,5** | 2100-2200 | 82,0 |
| Sm1_T11_profile3_20 | 101 | 312465 | 19,99776 | 717836 | 45,941504 | 1030301 | 65,939264 | **30,3** | 2200-2300 | 86,0 |
| | | | | | | | | | | |
| Sm1_T11_profile4_1 | 101 | 315258 | 20,176512 | 715043 | 45,762752 | 1030301 | 65,939264 | **30,6** | 200-300 | 10,0 |
| Sm1_T11_profile4_2 | 101 | 282955 | 18,10912 | 747346 | 47,830144 | 1030301 | 65,939264 | **27,5** | 300-400 | 14,0 |
| Sm1_T11_profile4_3 | 101 | 229430 | 14,68352 | 800871 | 51,255744 | 1030301 | 65,939264 | **22,3** | 400-500 | 18,0 |
| Sm1_T11_profile4_4 | 101 | 115683 | 7,403712 | 914618 | 58,535552 | 1030301 | 65,939264 | **11,2** | 500-600 | 22,0 |
| Sm1_T11_profile4_5 | 101 | 40797 | 2,611008 | 989504 | 63,328256 | 1030301 | 65,939264 | **4,0** | 600-700 | 26,0 |
| Sm1_T11_profile4_6 | 101 | 12101 | 0,774464 | 1018200 | 65,1648 | 1030301 | 65,939264 | **1,2** | 700-800 | 30,0 |
| Sm1_T11_profile4_7 | 101 | 11777 | 0,753728 | 1018524 | 65,185536 | 1030301 | 65,939264 | **1,1** | 800-900 | 34,0 |
| Sm1_T11_profile4_8 | 101 | 103348 | 6,614272 | 926953 | 59,324992 | 1030301 | 65,939264 | **10,0** | 900-1000 | 38,0 |
| Sm1_T11_profile4_9 | 101 | 152283 | 9,746112 | 878018 | 56,193152 | 1030301 | 65,939264 | **14,8** | 1000-1100 | 42,0 |
| Sm1_T11_profile4_10 | 101 | 236751 | 15,152064 | 793550 | 50,7872 | 1030301 | 65,939264 | **23,0** | 1100-1200 | 46,0 |
| Sm1_T11_profile4_11 | 101 | 244818 | 15,668352 | 785483 | 50,270912 | 1030301 | 65,939264 | **23,8** | 1200-1300 | 50,0 |
| Sm1_T11_profile4_12 | 101 | 306699 | 19,628736 | 723602 | 46,310528 | 1030301 | 65,939264 | **29,8** | 1300-1400 | 54,0 |
| Sm1_T11_profile4_13 | 101 | 222548 | 14,243072 | 807753 | 51,696192 | 1030301 | 65,939264 | **21,6** | 1400-1500 | 58,0 |
| Sm1_T11_profile4_14 | 101 | 238329 | 15,253056 | 791972 | 50,686208 | 1030301 | 65,939264 | **23,1** | 1500-1600 | 62,0 |
| Sm1_T11_profile4_15 | 101 | 240269 | 15,377216 | 790032 | 50,562048 | 1030301 | 65,939264 | **23,3** | 1600-1700 | 66,0 |
| Sm1_T11_profile4_16 | 101 | 320326 | 20,500864 | 709975 | 45,4384 | 1030301 | 65,939264 | **31,1** | 1700-1800 | 70,0 |
| Sm1_T11_profile4_17 | 101 | 241049 | 15,427136 | 789252 | 50,512128 | 1030301 | 65,939264 | **23,4** | 1800-1900 | 74,0 |
| Sm1_T11_profile4_18 | 101 | 298990 | 19,13536 | 731311 | 46,803904 | 1030301 | 65,939264 | **29,0** | 1900-2000 | 78,0 |
| Sm1_T11_profile4_19 | 101 | 277174 | 17,739136 | 753127 | 48,200128 | 1030301 | 65,939264 | **26,9** | 2100-2200 | 82,0 |
| Sm1_T11_profile4_20 | 101 | 314474 | 20,126336 | 715827 | 45,812928 | 1030301 | 65,939264 | **30,5** | 2200-2300 | 86,0 |

Data range

| | | |
|---|---|---|
| x | 100 | 200 |
| y | 400 | 500 |
| z | 200-2200 | |

| Data field | Dim. Pixel | Pores in | Pores | Rock in | Rock | Total volume | Total volume | Porosity | Data field | D. f. [z-in | |
|---|---|---|---|---|---|---|---|---|---|---|---|
| Unit | x*x*x | [pixelcounts] | in [mm³] | [pixelcounts] | in [mm³] | in [pixelcounts] | in [mm³] | in [%] | [z-Axis] | mm] | |
| Sm1_T11_profile5_1 | 101 | 370234 | 23,694976 | 660067 | 42,244288 | 1030301 | 65,939264 | **35,9** | 200-300 | 10,0 | Data range |
| Sm1_T11_profile5_2 | 101 | 300486 | 19,231104 | 729815 | 46,70816 | 1030301 | 65,939264 | **29,2** | 300-400 | 14,0 | x 275 375 |
| Sm1_T11_profile5_3 | 101 | 286735 | 18,35104 | 743566 | 47,588224 | 1030301 | 65,939264 | **27,8** | 400-500 | 18,0 | y 275 375 |
| Sm1_T11_profile5_4 | 101 | 222942 | 14,268288 | 807359 | 51,670976 | 1030301 | 65,939264 | **21,6** | 500-600 | 22,0 | z 200-2200 |
| Sm1_T11_profile5_5 | 101 | 174653 | 11,177792 | 855648 | 54,761472 | 1030301 | 65,939264 | **17,0** | 600-700 | 26,0 | |
| Sm1_T11_profile5_6 | 101 | 52089 | 3,333696 | 978212 | 62,605568 | 1030301 | 65,939264 | **5,1** | 700-800 | 30,0 | |
| Sm1_T11_profile5_7 | 101 | 52259 | 3,344576 | 978042 | 62,594688 | 1030301 | 65,939264 | **5,1** | 800-900 | 34,0 | |
| Sm1_T11_profile5_8 | 101 | 126732 | 8,110848 | 903569 | 57,828416 | 1030301 | 65,939264 | **12,3** | 900-1000 | 38,0 | |
| Sm1_T11_profile5_9 | 101 | 230619 | 14,759616 | 799682 | 51,179648 | 1030301 | 65,939264 | **22,4** | 1000-1100 | 42,0 | |
| Sm1_T11_profile5_10 | 101 | 254579 | 16,293056 | 775722 | 49,646208 | 1030301 | 65,939264 | **24,7** | 1100-1200 | 46,0 | |
| Sm1_T11_profile5_11 | 101 | 236949 | 15,164736 | 793352 | 50,774528 | 1030301 | 65,939264 | **23,0** | 1200-1300 | 50,0 | |
| Sm1_T11_profile5_12 | 101 | 266573 | 17,060672 | 763728 | 48,878592 | 1030301 | 65,939264 | **25,9** | 1300-1400 | 54,0 | |
| Sm1_T11_profile5_13 | 101 | 345451 | 22,108864 | 684850 | 43,8304 | 1030301 | 65,939264 | **33,5** | 1400-1500 | 58,0 | |
| Sm1_T11_profile5_14 | 101 | 348520 | 22,30528 | 681781 | 43,633984 | 1030301 | 65,939264 | **33,8** | 1500-1600 | 62,0 | |
| Sm1_T11_profile5_15 | 101 | 322511 | 20,640704 | 707790 | 45,29856 | 1030301 | 65,939264 | **31,3** | 1600-1700 | 66,0 | |
| Sm1_T11_profile5_16 | 101 | 340116 | 21,767424 | 690185 | 44,17184 | 1030301 | 65,939264 | **33,0** | 1700-1800 | 70,0 | |
| Sm1_T11_profile5_17 | 101 | 367856 | 23,542784 | 662445 | 42,39648 | 1030301 | 65,939264 | **35,7** | 1800-1900 | 74,0 | |
| Sm1_T11_profile5_18 | 101 | 364672 | 23,339008 | 665629 | 42,600256 | 1030301 | 65,939264 | **35,4** | 1900-2000 | 78,0 | |
| Sm1_T11_profile5_19 | 101 | 385785 | 24,69024 | 644516 | 41,249024 | 1030301 | 65,939264 | **37,4** | 2100-2200 | 82,0 | |
| Sm1_T11_profile5_20 | 101 | 382785 | 24,49824 | 647516 | 41,441024 | 1030301 | 65,939264 | **37,2** | 2200-2300 | 86,0 | |

| | Porosity in [%] | | |
|---|---|---|---|
| **AVERAGE** | **30,4** | 200-300 | 10,0 |
| | **27,9** | 300-400 | 14,0 |
| | **23,3** | 400-500 | 18,0 |
| | **16,6** | 500-600 | 22,0 |
| | **10,6** | 600-700 | 26,0 |
| | **2,6** | 700-800 | 30,0 |
| | **1,9** | 800-900 | 34,0 |
| | **7,9** | 900-1000 | 38,0 |
| | **16,2** | 1000-1100 | 42,0 |
| | **18,6** | 1100-1200 | 46,0 |
| | **20,1** | 1200-1300 | 50,0 |
| | **23,6** | 1300-1400 | 54,0 |
| | **25,7** | 1400-1500 | 58,0 |
| | **27,5** | 1500-1600 | 62,0 |
| | **29,0** | 1600-1700 | 66,0 |
| | **29,9** | 1700-1800 | 70,0 |
| | **30,2** | 1800-1900 | 74,0 |
| | **31,7** | 1900-2000 | 78,0 |
| | **29,8** | 2100-2200 | 82,0 |
| | **32,8** | 2200-2300 | 86,0 |

## *Minipermeameter*

## Sm1T11

Measurement report Minipermeameter

| | | | | |
|---|---|---|---|---|
| Date: | 280508 | **UniwienSM1T11** | | |
| Measuring gas: | N2 | | | |
| Gas - viscosity: | 0,0177 | Measuring pressure – reference: | 1,2 | bar a |
| Sensor: | 2 | Temperature: | 25,2 | °C |
| Tip radius: | 2,4 | Air pressure: | 1 | mbar |
| Geometric factor: | 4,9 | Contact pressure: | 8 | |

**Permeability**
**mD**

| | **-40** | **-30** | **-20** | **-10** | **0** | **10** | **y** |
|---|---|---|---|---|---|---|---|
| **40** | 267,38 | 684,65 | 159,09 | 340,57 | 163,2 | 177,01 | |
| **50** | 486,7 | 645,28 | 680,79 | 305,56 | 286,97 | 484,26 | |
| **60** | 479,97 | 549,84 | 386,44 | 597,57 | 711,93 | 1005,92 | |
| **70** | 254,79 | 291,76 | 580,08 | 503,71 | 500,89 | 231,34 | |
| **80** | 517,21 | 207,98 | 78,86 | 102,3 | 65,81 | 130,56 | |
| **90** | 202,76 | 200,5 | 673,36 | 809,69 | 659,41 | 91,13 | |
| **100** | 193,58 | 460,36 | 272,57 | 789,61 | 438,43 | 136,73 | |
| **110** | 387,43 | 266,69 | 222,01 | 421,74 | 69,79 | 35,15 | |
| **120** | 435,18 | 310,86 | 466,13 | 708,28 | 412,06 | 190 | |
| **130** | 348,27 | 851,16 | 463,46 | 408,91 | 419,1 | 183,96 | |
| **140** | 325,98 | 652 | 361,29 | 653,51 | 721,71 | 395,66 | |
| **150** | 408,91 | 674,98 | 415,51 | 572,68 | 695,51 | 348,47 | |
| **160** | 286,66 | 302,55 | 606,37 | 667,39 | 930,13 | 250,11 | |
| **170** | 718,13 | 604,9 | 1233,13 | 465,89 | 450,69 | 267,92 | |
| **180** | 196,74 | 113,48 | 232,1 | 65 | 427,81 | 63,41 | |
| **190** | 42,68 | 30,66 | 49,73 | 37,18 | 26,87 | 23,22 | |
| **200** | 8,61 | 8,41 | 5,53 | 8,2 | 8,26 | 7,82 | |
| **210** | 7,77 | 11,97 | 16,27 | 13,18 | 12,73 | 36,06 | |
| **220** | 319,99 | 25,61 | 42,22 | 398,39 | 83,15 | 511,77 | |
| **230** | 412,35 | 817,58 | 496,38 | 138,34 | 198,58 | 220,64 | |
| **240** | 232,98 | 344,34 | 600,9 | 323,38 | 364,77 | 336,1 | |
| **250** | 294,06 | 421,92 | 139,08 | 325,9 | 239,52 | 262,16 | |
| **260** | 339,34 | 182,13 | 312,41 | 208,38 | 209,79 | 177,7 | |
| **270** | 570,28 | 347,61 | 308,43 | 299,3 | 75,35 | 173,24 | |
| **x** | | | | | | | |

## Sm1T22

Measurement report Minipermeameter

| | | | | |
|---|---|---|---|---|
| Date: | 290508 | **UniwienSM1T22** | | |
| Measuring gas: | N2 | | | |
| Gas - viscosity: | 0,0177 | Measuring pressure – reference: | 1,2 | bar a |
| Sensor: | 2 | Temperature: | 24 | °C |
| Tip radius: | 2,4 | Air pressure: | 1 | mbar |
| Geometric factor: | 4,9 | Contact pressure: | 8 | |

**Permeability**
**mD**

| | **-40** | **-30** | **-20** | **-10** | **0** | **10** | **y** |
|---|---|---|---|---|---|---|---|
| **40** | 207,88 | 267,04 | 88,77 | 26,82 | 48,2 | 12,05 | |
| **50** | 57,3 | 140,38 | 108,64 | 49,87 | 69,76 | 82,35 | |
| **60** | 427,65 | 115,19 | 119,54 | 156,84 | 59,79 | 106,35 | |
| **70** | 57,36 | 92,08 | 163,72 | 414,22 | 145,88 | 190,63 | |
| **80** | 30,01 | 13,45 | 31,71 | 98,83 | 295,42 | 84,7 | |
| **90** | 143,11 | 99,92 | 64,09 | 50,38 | 15,94 | 25,54 | |
| **100** | 73,45 | 81,28 | 47,04 | 78,7 | 51,21 | 61,52 | |
| **110** | 99,23 | 48,31 | 54,87 | 25,77 | 60,5 | 50,59 | |
| **120** | 161,98 | 53,49 | 34,3 | 39,72 | 36,17 | 73,59 | |
| **130** | 45,67 | 24,01 | 45,48 | 26,05 | 50,68 | 29,13 | |
| **140** | 48,43 | 79,32 | 26,07 | 46,72 | 27,83 | 39,35 | |
| **150** | 70,3 | 33,32 | 25,09 | 39,92 | 24,59 | 22,55 | |
| **160** | 28,01 | 31,6 | 40,26 | 24,01 | 21,58 | 40,99 | |
| **170** | 166,53 | 51,56 | 22,37 | 25,21 | 21,51 | 31,38 | |
| **180** | 312,8 | 92,35 | 61,15 | 30,73 | 19,42 | 22,98 | |
| **185** | 173,21 | 122,45 | 53,56 | 52,8 | 30,96 | 16,72 | |
| **190** | 153,3 | 232,53 | 62,78 | 127,09 | 125,51 | 50,02 | |
| **195** | 12,01 | 20,1 | 52,3 | 499,43 | 118,2 | 35,9 | |
| **200** | 5,77 | 4,57 | 3,85 | 12,12 | 5,05 | 7,79 | |
| **205** | 3,94 | 4,38 | 4,37 | 4,49 | 4,06 | 4,14 | |
| **210** | 10,21 | 8,17 | 4,33 | 4,71 | 5,06 | 4,36 | |
| **215** | 34,4 | 14,26 | 87,42 | 27,68 | 5,77 | 6,09 | |
| **220** | 54 | 64,14 | 115,04 | 27,73 | 40,23 | 19,68 | |
| **225** | 134,96 | 133,03 | 47,81 | 44,58 | 44,35 | 15,34 | |
| **230** | 68,88 | 105,49 | 117,22 | 21,78 | 138,82 | 23,83 | |
| **240** | 115,35 | 85,51 | 104,08 | 102,07 | 29,39 | 45,57 | |
| **250** | 182,98 | 66,22 | 152,9 | 111,3 | 97,59 | 35,52 | |
| **260** | 119,06 | 99,19 | 117,06 | 124,52 | 130,56 | 197,4 | |

**x**

## Sm2T12

Measurement report Minipermeameter

| | | | | |
|---|---|---|---|---|
| Date: | 300508 | **UniwienSM2T12** | | |
| Measuring gas: | N2 | | | |
| Gas - viscosity: | 0,0177 | Measuring pressure – reference: | 1,2 | bar a |
| Sensor: | 2 | Temperature: | 24 | °C |
| Tip radius: | 2,4 | Air pressure: | 1 | mbar |
| Geometric factor: | 4,9 | Contact pressure: | 8 | |

**Permeability**
**mD**

| | **-40** | **-30** | **-20** | **-10** | **0** | **10** | **y** |
|---|---|---|---|---|---|---|---|
| **20** | 781,32 | 571,42 | 313,09 | 408,62 | 233,39 | 798,13 | |
| **30** | 245,35 | 758,99 | 519,23 | 433,8 | 352,9 | 410,45 | |
| **40** | 536,95 | 376,07 | 427,52 | 617,38 | 837,07 | 731,91 | |
| **50** | 394,26 | 268,98 | 293,53 | 611,48 | 286,62 | 496,77 | |
| **60** | 848,79 | 284,6 | 108,5 | 101,49 | 64,18 | 224,03 | |
| **70** | 329,51 | 506,33 | 160,45 | 118,6 | 164,4 | 188,5 | |
| **80** | 531,9 | 192,98 | 460,36 | 1007,51 | 493,14 | 437,72 | |
| **90** | 474,01 | 272,63 | 1200,03 | 953,1 | 572,75 | 322,78 | |
| **100** | 177,09 | 354,22 | 1579,64 | 189,01 | 40,97 | 20,86 | |
| **110** | 36,48 | 166,34 | 65,28 | 34,1 | 30,64 | 27,58 | |
| **120** | 31,15 | 28,14 | 34,2 | 46,15 | 45,54 | 107,42 | |
| **130** | 67,21 | 41,7 | 36,93 | 39,58 | 51,08 | 53,92 | |
| **140** | 169,4 | 155,45 | 57,87 | 45,69 | 48,99 | 46,89 | |
| **150** | 122,85 | 70,18 | 53,72 | 65,15 | 53,61 | 58,16 | |
| **160** | 187,8 | 724,42 | 802,23 | 113,87 | 157,68 | 102,84 | |
| **170** | 1913,04 | 1155,56 | 303,4 | 77,73 | 261,44 | 364,92 | |
| **180** | 711,75 | 948,73 | 241,91 | 873,7 | 694,23 | 373,94 | |
| **190** | 880,52 | 574,12 | 667,47 | 366,24 | 551,69 | 686,65 | |
| **200** | 2004,15 | 719,06 | 522,93 | 556,8 | 230,99 | 582,53 | |
| **210** | 1048,56 | 498,64 | 539,77 | 305,17 | 237,84 | 555,66 | |
| **220** | 825,85 | 1093,63 | 316,13 | 263,22 | 147,87 | | |
| **230** | 728,24 | 763,32 | 339,95 | 252,56 | 320,45 | 864,02 | |
| **x** | | | | | | | |

## Sm2T22

Measurement report Minipermeameter

| | | | | |
|---|---|---|---|---|
| Date: | 280508 | **UniwienSM2T22** | | |
| Measuring gas: | N2 | | | |
| Gas - viscosity: | 0,0177 mPas | Measuring pressure – reference: | 1,2 | bar a |
| Sensor: | 2 | Temperature: | 24 | °C |
| Tip radius: | 2,4 mm | Air pressure: | 1 | mbar |
| Geometric factor: | 4,9 | Contact pressure: | 8 | |

**Permeability mD**

| | **-40** | **-30** | **-20** | **-10** | **0** | **10** | **y** |
|---|---|---|---|---|---|---|---|
| **10** | 3167,37 | 1774,57 | 745,3 | 725,72 | 1873,74 | 2000,3 | |
| **20** | 2019,5 | 2647,56 | 1045,99 | 880,67 | 2945,85 | 870,7 | |
| **30** | 2019,5 | 2791,69 | 2039,59 | 764,62 | 617,6 | 641,77 | |
| **40** | 2294,12 | 1965,82 | 2490,42 | 860,01 | 708,79 | 1063,42 | |
| **50** | 2053,98 | 2102,9 | 801,99 | 637,11 | 616,39 | 557,2 | |
| **60** | 2053,98 | 2133,21 | 729,63 | 802,86 | 557,84 | 646,48 | |
| **70** | 2447,59 | 918,71 | 1081,79 | 1000 | 648,15 | 591,04 | |
| **80** | 731,87 | 1120,02 | 825,28 | 1924,78 | 787,54 | 1979,8 | |
| **90** | 2333,42 | 749,05 | 725,02 | 1042,4 | 687,79 | 900,56 | |
| **100** | 2186,78 | 1081,11 | 646,24 | 828,47 | 425,89 | 358,3 | |
| **110** | 817,32 | 313,02 | 325,88 | 399,96 | 102,75 | 147,65 | |
| **120** | 272,31 | 2352,17 | 1072,25 | 782,05 | 538,66 | 292,23 | |
| **130** | 315,46 | 744,24 | 2508,1 | 2181,8 | 497,62 | 262,36 | |
| **140** | 1,78 | 33,58 | 4,55 | 82,53 | 107,58 | 46,66 | |
| **150** | 2,84 | 4,6 | 1,31 | 1,1 | 0 | 0 | |
| **160** | 3,4 | 5,42 | 4,76 | 35,02 | 5,52 | 4,33 | |
| **170** | 157,47 | 156,53 | 11,7 | 21,45 | 61,23 | 21,09 | |
| **180** | 19,86 | 133,11 | 247,21 | 80,6 | 62,45 | 44,06 | |
| **190** | 787,3 | 1193,46 | 710,87 | 2560,13 | 809,17 | 100,04 | |
| **200** | 1017,14 | 845,03 | 588,27 | 2337,75 | 2180,83 | 618,12 | |
| **x** | | | | | | | |

## Sm3

Measurement report Minipermeameter

| | | | | |
|---|---|---|---|---|
| Date: | 280508 | **UniwienSM3T11** | | |
| Measuring gas: | N2 | | | |
| Gas - viscosity: | 0,0177 | Measuring pressure – reference: | 1,2 | bar a |
| Sensor: | 2 | Temperature: | 25,2 | °C |
| Tip radius: | 2,4 | Air pressure: | 1 | mbar |
| Geometric factor: | 4,9 | Contact pressure: | 8 | |

**Permeability**
**mD**

| | **-40** | **-30** | **-20** | **-10** | **0** | **10** | **y** |
|---|---|---|---|---|---|---|---|
| **40** | 11,02 | 4,19 | 9,94 | 15,31 | 16,07 | 22,84 | |
| **50** | 32,19 | 21,32 | 23,9 | 24,36 | 13,8 | 18,44 | |
| **60** | 21,46 | 44,56 | 21,01 | 19,07 | 10,82 | 23,58 | |
| **70** | 13,56 | 25,71 | 18,63 | 16,62 | 14,96 | 30,45 | |
| **80** | 14,19 | 30,19 | 21,3 | 23,58 | 16,62 | 33,88 | |
| **90** | 30,86 | 29,12 | 22,62 | 23,56 | 17,59 | 45,83 | |
| **100** | 31,38 | 17,22 | 29,6 | 13,24 | 16,95 | 17,89 | |
| **110** | 11,24 | 9,33 | 12,44 | 12,24 | 18,6 | 66,2 | |
| **120** | 26,27 | 21,12 | 13,98 | 18,6 | 17,5 | 12,28 | |
| **130** | 13,09 | 18,47 | 17,37 | 15,37 | 11,42 | 14,53 | |
| **140** | 10,12 | 16,25 | 9,23 | 9,53 | 10,18 | 11,63 | |
| **150** | 14,11 | 18,78 | 11,17 | 21,8 | 11,02 | 9,28 | |
| **160** | 15,2 | 10,67 | 14,96 | 22,13 | 11,12 | 11,62 | |
| **170** | 17,04 | 13,11 | 15,57 | 14,16 | 16,08 | 13,23 | |
| **180** | 19,8 | 19,93 | 13,78 | 16,32 | 14,49 | 9,32 | |
| **190** | 12,88 | 11,11 | 10,65 | 12,57 | 15,94 | 14,4 | |
| **200** | 14,88 | 13,41 | 14,77 | 18,13 | 14,75 | 15,26 | |
| **210** | 14,77 | 11,93 | 10,88 | 17,33 | 21,8 | 789,53 | |
| **220** | 15,18 | 16,94 | 10,16 | 11,85 | 14 | 16,92 | |
| **230** | 11,65 | 25,51 | 29,2 | 29,84 | 21,91 | 20,61 | |
| **240** | 124,46 | 20 | 22,82 | 24,64 | 28,17 | 33,94 | |
| **250** | 77,54 | 34,83 | 25,9 | 39,11 | 38,61 | 25,91 | |
| **260** | 31,81 | 35,7 | 96,43 | 32,67 | 27,6 | 14,32 | |
| **270** | 32,44 | 59,7 | 62,59 | 510,83 | 106,8 | 25,3 | |
| **280** | 16,53 | 20,4 | 56,88 | 15,84 | 13,41 | 19,52 | |
| **290** | 15,16 | 15,5 | 12,16 | 8,35 | 10,46 | 190,23 | |
| **300** | 16,13 | 6,89 | 11,27 | 44,08 | 29,28 | 23,87 | |
| **310** | 47,34 | 19,01 | 16,9 | 20,22 | 20,16 | 17,38 | |
| **320** | 10,72 | 18,3 | 14,76 | 16,35 | 15,94 | 15,22 | |
| **330** | 15,5 | 15,14 | 14,67 | 18,68 | 15,48 | 16,09 | |
| **340** | 15,52 | 14,77 | 17,09 | 18,28 | 16,03 | 23,77 | |
| **350** | 23,99 | 19,84 | 21,09 | 28,17 | 18,44 | 31,42 | |
| **360** | 24,48 | 14,66 | 21,53 | 17,75 | 28,31 | 19,52 | |

| | | | | | | |
|---|---|---|---|---|---|---|
| **370** | 15,03 | 8,45 | 8,02 | 11,32 | 11,42 | 11,91 |
| **380** | 8,75 | 11,72 | 12,05 | 38,05 | 23,18 | 13,38 |
| **390** | 10,83 | 6,54 | 10,58 | 9,17 | 12,66 | 10,4 |
| **400** | 8,36 | 9,81 | 12 | 10,49 | 10,01 | 15,18 |
| **410** | 37,07 | 19,46 | 10,71 | 8,95 | 10,44 | 11,42 |
| **420** | 15,06 | 15,57 | 19,09 | 84,08 | 22,28 | 105,86 |
| **430** | 16,99 | 26,26 | 21,4 | 18,68 | 21,67 | 21,89 |
| **440** | 19,5 | 29,27 | 21,85 | 34,9 | 31,77 | 22,51 |
| **450** | 15,61 | 14,94 | 18,87 | 22,2 | 17,87 | 24,55 |
| **460** | 21,9 | 17,99 | 16,07 | 14,61 | 11,48 | 17,29 |
| **x** | | | | | | |

## Sm7

Measurement report Minipermeameter

| | | | | |
|---|---|---|---|---|
| Date: | 290508 | **UniwienSM7-Wdhg** | | |
| Measuring gas: | N2 | | | |
| Gas - viscosity: | 0,0177 | Measuring pressure – reference: | 1,2 | bar a |
| Sensor: | 2 | Temperature: | 24 | °C |
| Tip radius: | 2,4 | Air pressure: | 1 | mbar |
| Geometric factor: | 4,9 | Contact pressure: | 8 | |

**Permeability mD**

| | **-40** | **-30** | **-20** | **-10** | **0** | **10** | **y** |
|---|---|---|---|---|---|---|---|
| **0** | 51,32 | 62,14 | 61,97 | 64,14 | 63,98 | 44,42 | |
| **10** | 53,62 | 84,76 | 88,05 | 94,27 | 91,42 | 67,11 | |
| **20** | 71,97 | 30,51 | 109,66 | 153,59 | 138,73 | 71,99 | |
| **30** | 33,61 | 52,28 | 87,95 | 163,56 | 102,7 | 150,55 | |
| **40** | 73,47 | 113,07 | 107,14 | 186,42 | 139,87 | 75,37 | |
| **50** | 6,73 | 5,16 | 4,4 | 4,28 | 4,37 | 3,71 | |
| **60** | 77,3 | 84,88 | 196,01 | 155,93 | 166,06 | 147,2 | |
| **70** | 99,87 | 104,33 | 175,72 | 111,48 | 225,08 | 223,2 | |
| **80** | 108,55 | 207,1 | 90,4 | 75,52 | 128,74 | 116,83 | |
| **90** | 114,82 | 44,91 | 95,78 | 66,58 | 109,51 | 63,41 | |
| **100** | 100,93 | 48,3 | 131,01 | 35,75 | 36,63 | 64,19 | |
| **110** | 72,32 | 135,66 | 43,12 | 21,64 | 33,54 | 33,79 | |
| **x** | | | | | | | |

## Sm9

Measurement report Minipermeameter

| | | | | |
|---|---|---|---|---|
| Date: | 290508 | **UniwienSM9** | | |
| Measuring gas: | N2 | | | |
| Gas - viscosity: | 0,0177 | Measuring pressure – reference: | 1,2 | bar a |
| Sensor: | 2 | Temperature: | 24 | °C |
| Tip radius: | 2,4 | Air pressure: | 1 | mbar |
| Geometric factor: | 4,9 | Contact pressure: | 8 | |

**Permeability**
**mD**

| | **-40** | **-30** | **-20** | **-10** | **0** | **10** | **y** |
|---|---|---|---|---|---|---|---|
| **60** | 7,57 | 11,39 | 10,13 | 18,73 | 36,96 | 37,28 | |
| **70** | 34,78 | 22,72 | 26,43 | 31,32 | 35,56 | 32,41 | |
| **80** | 29,25 | 31,94 | 34,56 | 42,36 | 30,79 | 35,25 | |
| **90** | 54,46 | 43,91 | 37,07 | 23,98 | 38,21 | 41,2 | |
| **100** | 114,94 | 24,22 | 34,92 | 38,65 | 35,75 | 30,41 | |
| **110** | 33,55 | 33,44 | 54,48 | 33,9 | 30,26 | 32,81 | |
| **120** | 27,74 | 28,21 | 32,54 | 37,94 | 42,96 | 25,15 | |
| **130** | 25,13 | 21,06 | 23,6 | 29,9 | 17,55 | 15,09 | |
| **140** | 11,61 | 4,68 | 10,66 | 16,14 | 15,66 | 27,9 | |
| **150** | 21,5 | 22,15 | 21,9 | 28,52 | 23,8 | 32,54 | |
| **160** | 29,02 | 28,83 | 27,56 | 25,37 | 26,94 | 23,54 | |
| **170** | 21,3 | 20,89 | 18,81 | 22,25 | 26,67 | 59,83 | |
| **180** | 40,33 | 20,37 | 19,67 | 20,98 | 22,88 | 23,87 | |
| **190** | 33,28 | 21,3 | 27,8 | 18,77 | 21,88 | 24,89 | |
| **200** | 44,44 | 36,13 | 21,48 | 24,87 | 24,57 | 35,14 | |
| **210** | 31,17 | 25,37 | 26,29 | 27,77 | 20,78 | 19,47 | |
| **x** | | | | | | | |

## Sm10

Measurement report Minipermeameter

| | | | | |
|---|---|---|---|---|
| Date: | 290508 | **UniwienSM10** | | |
| Measuring gas: | N2 | | | |
| Gas - viscosity: | 0,0177 | Measuring pressure – reference: | 1,2 | bar a |
| Sensor: | 2 | Temperature: | 24 | °C |
| Tip radius: | 2,4 | Air pressure: | 1 | mbar |
| Geometric factor: | 4,9 | Contact pressure: | 8 | |

**Permeability**
**mD**

| | **-30** | **-25** | **-20** | **-15** | **-10** | **-15** | **0** | **5** | **10** | **y** |
|---|---|---|---|---|---|---|---|---|---|---|
| **30** | 140,44 | | 129,26 | | 204,92 | | 199,91 | | 351,12 | |
| **40** | 54,85 | | 13,6 | | 74,89 | | 119,67 | | 125,99 | |
| **50** | 5,58 | | 4,51 | | 37,69 | | 208,51 | | 76,37 | |
| **60** | 4,87 | | 4,91 | | 107,76 | | 26,57 | | 145,42 | |
| **70** | 38,69 | | 12,47 | | 49,41 | | 8,89 | | 5,96 | |
| **80** | 165,24 | | 4,73 | | 24,84 | | 108,42 | | 66,75 | |
| **90** | 42,32 | | 103,26 | | 157,26 | | 122,83 | | 126,41 | |
| **100** | 247,38 | | 355,84 | | 11,52 | | 203,01 | | 323,05 | |
| **110** | 40,99 | | 107,06 | | 106,65 | | 121,58 | | 204,38 | |
| **120** | 18,51 | | 9,98 | | 27,57 | | 44,34 | | 125,56 | |
| **130** | 107,83 | | 34,12 | | 295,62 | | 554,09 | | | |
| **140** | 196,99 | | 672,41 | | 513,08 | | 42,35 | | 232,36 | |
| **150** | 641,32 | | 922,96 | | 329,1 | | 28,22 | | 1,3 | |
| **160** | 57,81 | 149,6 | 41,44 | 58,92 | 26,92 | 10,69 | 12,34 | 6,27 | 10,26 | |
| **165** | 3,09 | 4,32 | 5,68 | 8,74 | 8,04 | 9,07 | 17,48 | 17,7 | 12,2 | |
| **170** | 6,24 | 6,89 | 5,24 | 5,53 | 4,51 | 6,79 | 7,6 | 4,66 | 4,76 | |
| **175** | 4,77 | 4,45 | 4,31 | 4,23 | 4,2 | 4,16 | 4,05 | 4,04 | 4,02 | |
| **180** | 3,82 | 3,82 | 3,77 | 3,76 | 3,74 | 3,75 | 3,78 | 3,83 | 4 | |
| **185** | 3,37 | 3,72 | 3,74 | 3,74 | 3,76 | 4,03 | 6,05 | 14,2 | 8,85 | |
| **190** | | 1,88 | 0,54 | 0,2 | 1,66 | 1,22 | 6,51 | 1,45 | 7,52 | |
| **195** | 0 | 0,01 | 0,05 | 6,09 | 160,69 | 249,95 | 526,07 | 305,03 | 274,75 | |
| **200** | 2,93 | 69,36 | 209,33 | 532,15 | 329,17 | 261,24 | 280,4 | 788,28 | 94,77 | |
| **205** | 101,64 | 113,05 | 205,08 | 103,1 | 468,6 | 249,33 | 1227,72 | 887,17 | 485,06 | |
| **210** | 431,2 | 27,04 | 103,35 | 561,51 | 868,63 | | 885,95 | 1017,79 | 648,21 | |
| **220** | 602,39 | | | | 1187,05 | | 967,69 | | 810,86 | |
| **230** | 630,57 | | | | 805,66 | | 859,09 | | 693,98 | |
| **240** | 877,87 | | | | 947,39 | | 810,46 | | 375,26 | |
| **250** | 673,73 | | | | 711,42 | | 507,92 | | 551,39 | |
| **260** | 730,36 | | | | | | 708,82 | | 587,54 | |
| **270** | 540,93 | | 885,11 | | 594,11 | | 780,77 | | 857,88 | |
| **x** | | | | | | | | | | |

## *ACKNOWLEDGEMENT*

First of all I would like to thank my supervisors Ulrike Exner and Bernhard Grasemann (University of Vienna), for supporting me in an extraordinary way in all parts of this work, especially Ulrike Exner who had always time for questions and discussions. Their guidance and support helped me through every step of my master thesis and assisted me to improve it to reach the final result.

Many thanks to Erich Draganits, who discovered the deformation bands in the Leitha limestone as he worked at Vienna University of Technology, for providing information and starting the research on the very interesting topic.

I gratefully acknowledge Clemens Jülinger (quarry HUMMEL) for providing rock samples and for permitting access to the quarry.

Big thanks to the team of the Department of Anthropology (University of Vienna), especially to Martin Dockner (IT-Technician) and Gerhard Weber (Deputy Head at the Department of Anthropology) for being able to work with the µCT and for providing helpful information and discussions.

Electron microprobe measurements were performed at the Department of Lithospheric Research. Acquisition of BSE images and element maps, as well as interpretation and discussion by Cornelius Tschegg is gratefully acknowledged.

Best regards to OMV LEP-FC for providing me with minipermeameter analysis and routine core analysis (PoroPerm) measurements of my used drill cores.

I am greatly indebted to Richard Laner who relinquished his data of his Bachelor paper to me, which was essential for this master thesis.

Many thanks to all my colleagues in my semester, Nikolaus Bartl, Bernhard Bretis, Christine Dunkel, Vanessa Fremd, Jürgen Leitner, Hans Reitinger, Christian Schrott, Jonas Weil and Magdalena Bottig, Marcel Frehner for supporting and having a lot of fun during excursion and our years of study.

Furthermore I would like to thank all from the Center of Earth Sciences for helping and giving support.

I am deeply indebted to my whole family that made my enjoyable studying years possible, not at least with their financial support but also for supporting and providing confidence and trust.

Finally a warm and hearty “Thank You” to Kati for your love and trust and the time we spend together. You gave me support in every situation of life.

## *LIST OF FIGURES*

## *CURRICULUM VITAE*

### Personal Data


| | |
|---|---|
| Name: | Alexander Rath |
| Date of birth: | 9. Oktober 1985 |
| Place of birth: | Mödling |
| Family status: | single |
| Nationality: | Austria |
| Adress: | Babenbergerstraße 6, 2500 Baden |
| E-mail: | alexrath@gmx.net |


### Education

| | |
|---|---|
| 02. 2008 – 03. 2010 | Master study Geology, Uni. Wien |
| 10. 2004 – 02. 2008 | Bachelor study in Earth sciences, Uni. Wien |
| 01.-08. 2004 | Military Service, Baden |
| 10. 1995 – 06. 2003 | High school:BG & BRG Biondekgasse, Baden |
| 10. 1991 – 06. 1995 | Elementary school: Radetzkystraße, Baden |

### Work experience additionally to the academic study

| | |
|---|---|
| 10. 2009 - | Alpenverein: Climbing for kids (voluntary) |
| 07. + 10.-12. 2008 | GeoExpert GmbH. Internship |
| 08. 2007 - | Natural History Museum Wien (Mineralogy) |
| 10.2003 – 07. 2007 | SR-Archiv |

### Tutor

| | |
|---|---|
| SS 2009 | Geological mapping (in the area of Schönfeld(Sbg)) |
| WS 2008 | Quatification of geological processes |
| SS 2008 | Structural Geology and Tectonics (Excursion to Spain) |

### Special Experience

2002 Exchange semester Quincy, IL, USA during Junior Highschool Year

### Scholarhips

OMV Conference Grant 2009
Scholarship from the University of Vienna, financed by Bmwf. Study year: 2009

### Excursion guides

Rath, A., Exner, U., Grasemann, B. & Draganits, E. (2008). Deformation Bands in the unconsolidated sands and gravels of the sand pit St. Georgen, Burgenland Exkursion E2, Pangeo Austria 2008, 23.-24. September 2006, Excursion guide.

### Abstracts

A. Rath, U. Exner, B. Grasemann, R. Laner, D. Köhn, J.-O. Schwarz, L. Huber, F. Kerschner. Changes of petrophysical properties in deformation bands (Leithakalk, Eastern Austria). Geophysical Research Abstracts, Vol. 11, EGU2009-0, 2009

Rath, A., Laner, R., Exner, U., Grasemann, B., Philippovich, N., Kerschner, F. (2008): Quantitative analysis of deformation bands in porous sediments in the Eisenstadt Basin, Austria. Pangeo Austria 2008, 23.-24. September 2006, abstract volume, Mitteilungen der Gesellschaft der Geologie- und Bergbaustudenten in Österreich, 49.

Rath, A., Exner, U., Grasemann, B., Draganits, E. (2008) Deformation bands in non-consolidated sediments (Eisenstadt Basin, Austria). Geophysical Research Abstracts, Vol. 10.

## Presentations

OMV Technology Platform 25.02.2010
Pangeo 2008 Wien
OMV EOC Day 2009 Wien
Tectonomechanics Colloquium Salzburg 2009